ELASTIC SCATTERING OF PROTONS BY CARBON 12 AND CARBON 13

Thesis by

Edmund Alexander Milne

In Partial Fulfillment of the Requirements

for the Degree of

Doctor of Philosophy

CALIFORNIA INSTITUTE OF TECHNOLOGY

Pasadena, California

1953

ACKNOWLEDGMENTS

I wish to express my gratitude to Dr. W.A. Fowler for suggesting and supervising this problem and to Dr. C.C. Lauritsen and Dr. R.F. Christy for their comments and suggestions on this work.

I wish to express my thanks to Mr. W.D. Warters, Dr. W.A. Fowler, and Dr. C.C. Lauritsen for their assistance in operating the Van de Graaff generator and in obtaining the data.

This work was assisted by the joint program of the ONR and AEC.

ABSTRACT

A determination of the differential cross section for the elastic scattering of protons by carbon twelve at angles of every ten degrees in the center of mass system from 30 to 160 degrees has been made near the 460 kev resonance in $C^{12}(p\gamma)$. A phase shift analysis of the carbon twelve data has been performed.

The differential cross section for the elastic scattering of protons by carbon thirteen has been determined in the energy range from 450 kev to 1.6 mev at angles of 50, 90, 120, and 160 degrees in the center of mass system. Anomalies were found in the scattering at 0.556, 1.158, 1.465, and 1.550 mev. A qualitative discussion is presented on these states in the compound nucleus, nitrogen fourteen.

An electrostatic generator was used to produce a beam of protons of accurately known energy. A double focusing, variable angle, magnetic, proton spectrometer was used to obtain a momentum analysis of the scattered particles. A magnetometer and magnet control circuit for the spectrometer are discussed.

TABLE OF CONTENTS

PART I

INTRODUCTION

One of the many branches of nuclear physics has to do with the study of the excited states in the light nuclei. Among the important properties of these excited states are the energy, width, parity and spin. Information about some of these states can be obtained from elastic scattering experiments, since the scattering depends on the spins and parities of the states of the intermediate nucleus as well as on the relative angular momentum of the interacting particles.

Although a partial wave analysis of scattering data often yields definite values for the spins and parities, it is usually quite difficult to perform, especially if the particles have spin and if several phase shifts are involved. However, many inferences can be drawn from the shapes of the scattering curves at various angles. The states investigated here are the 2.37 mev level in N^{13} produced in the bombardment of C^{12} by protons and the 8.06, 8.62, 8.70, 8.90 and 8.98 mev levels in N^{14} produced in the bombardment of C^{13} by protons.

PART II

EXPERIMENTAL EQUIPMENT

The data for the elastic scattering of protons by C^{12} was obtained by using the electrostatic generator constructed in 1938 (1) and partially reconstructed in 1946. Even though this machine was still in working order, considerable maintenance, particularly of the vacuum system, was necessary to keep it in operation. The maximum obtainable voltage had decreased from 1.7 mev to about 1.4 mev.

In the summer of 1952 this machine was rebuilt by the author and Mr. W.D. Warters. The structural design was not essentially changed; there are four supporting columns for the high potential electrode with a single vacuum tube in the middle. The vacuum tube was replaced by one similar to those in the other two generators in Kellogg Radiation Laboratory. It differs from them in that it is made in sections. These sections are bolted together with two concentric "O"-ring vacuum seals at each joint. The space between the "O"-rings can be pumped out through a pump out hole. This enables one to check the "O"-rings for leaks. The sections are made of seven porcelain insulators and electrodes. The ends of the insulators were lapped to the electrodes, and the lapped surfaces were then painted with vinylite. The insulators and electrodes were then baked to drive out all of the solvent in the vinylite; the insulators and electrodes were then put together and

rebaked. This made the sections strong and vacuum tight.

The ion source was not replaced, but the voltage and power supply for the ion source were completely rewired and the components replaced. Moreover, the ion source generator receives its power now from the top roller of the main charging belt; whereas before it had a separate motor and drive belt.

The new charging belt motor is a five horsepower, three phase, induction motor. It was placed at the bottom of the machine inside the pressure tank, eliminating the old jack-shaft and seal necessary when the motor was on the outside of the tank.

The machine now runs much more quietly than before. It has required very little maintenance to keep it in operation. The maximum obtainable voltage is now about 2.1 mev. All of the C^{13} data and some of the C^{12} data was obtained from the rebuilt machine.

The protons from the electrostatic generator are analyzed by an 80 degree electrostatic analyzer. It was built especially for use with the magnetic spectrometer described below. The analyzer is shielded by a steel pipe from the stray field of the magnetic spectrometer. The analyzer was calibrated on the 993.3 kev resonance in the Al^{27} $(p\gamma)$ reaction.

The double focusing, magnetic, proton spectrometer previously described[2] has been remounted so as to allow a continuously variable scattering angle from 0 to 160 degrees[3]. The spectrometer, suspended between the ceiling and the floor,

rotates about a vertical axis through the center of the target chamber. The arrangement is shown in Figure 1A*.

The target chamber, shown in Figure 1B, is made in two parts. The bottom half is rigidly connected to the vacuum chamber of the spectrometer, and the top half is supported by the diffusion pump, and is connected to the electrostatic analyzer through a sylphon bellows. The two parts of the target chamber can rotate with respect to each other on an "O"-ring seal. The protons enter the target chamber at an angle of ten degrees with the horizontal, just grazing the bottom of the entrance channel. The proton beam passes through a steel pipe for magnetic shielding between the analyzer and the target chamber. This pipe is inside the vacuum system of the entrance channel. The scattered protons that enter the spectrometer leave the target at an angle of ten degrees and just graze the top of the exit channel.

---

* For a more detailed description of the spectrometer and target chamber see W.D. Warters Ph. D. Thesis, California Institute of Technology (1953).

PART III

MAGNETOMETER

The momentum P of a particle of charge ze and rest mass M_o moving in a magnetic field B with radius of curvature ρ is given by

$$Pc = zeB\rho \quad . \tag{1}$$

The energy E of this particle is given by

$$E = \sqrt{P^2c^2 + (M_oc^2)^2} \quad - M_oc^2 \tag{2}$$

$$= M_oc^2\left[\sqrt{\left(\frac{zeB\rho}{M_oc^2}\right)^2 + 1} \quad - 1\right]$$

$$\doteq \frac{(Bze\rho)^2}{2M_oc^2}\left[1 - \frac{1}{4}\left(\frac{Bze\rho}{M_oc^2}\right)^2 + \cdots\right] . \tag{3}$$

If one designates the non-relativistically calculated energy as E_o, where

$$E_o = \frac{(Bze\rho)^2}{2M_oc^2} \tag{4}$$

equation (3) becomes

$$E \doteq E_o(1 - E_o/2M_oc^2). \tag{5}$$

The term in the bracket is the relativistic correction. One obtains the same expression for the correction for the electrostatic analyzer except the sign is plus. For protons of energy less than 2 mev this correction is at most 0.1 per cent.

To measure E one must measure ρ and B. The radius of curvature ρ was fixed by the spectrometer exit slits and the target, and the relative values of B were measured with a magnetometer. This consisted of a coil carrying a current I suspended in the magnetic field. The coil had a restoring torque which just balanced the torque produced by the field acting on the coil. Thus we have

$$BI = \text{a constant}$$

and from equation (4)

$$EI^2 = kZ/M \tag{6}$$

where k is the magnetometer constant. For protons

$$EI^2 = k_p = k/M_p. \tag{7}$$

The magnetometer should be able to measure the relative magnetic field to an accuracy of the order of 1/10th the resolution of the spectrometer. It also is convenient to have an automatic field regulator to keep the magnetic field constant during a run. For narrow resonances the field must be kept very constant during the run.

The magnetometer previously described [4] could not be used with the new mounting of the spectrometer without being rebuilt. Besides this, it used a phosphor bronze spring to apply the restoring torque. This was unsatisfactory because of hysteresis and a drift in the spring that limited its accuracy.

Because of this hysteresis and drift in the phosphor bronze spring other materials were investigated. Since the spring was to be placed in the magnetic field no magnetic materials could be used. All of the other metals that were tried were unsatisfactory. Both Dr. C.C. Lauritsen and Dr. John Seagrave suggested that a quartz fiber might be better than metal springs for applying the restoring torque to the coil. Quartz fibers were then made using the technique developed by Professor H.V. Neher [5].

Quartz proved to have many advantages. The viscosity is only 10^{-3} of that in the best metals[5]. The temperature coefficient of the rigidity modulus is 1.3×10^{-4} per degree centigrade, while that measured for phosphor bronze is 6×10^{-4} per degree centigrade. The coefficient of thermal expansion of quartz is very low. The hysteresis of the phosphor bronze spring is of the order of 0.4 per cent while that of the quartz fiber is less than 0.05 per cent.

The coil was made by winding 16 turns of no. 32 copper wire on a lucite bobbin. The coil assembly is shown in Figure 2. Inside the bobbin there is an aluminum ring for magnetic damping of the coil. The weight of the coil is supported by a ten mil tungsten wire fastened to the top of the coil and resting in a jewel bearing. A phosphor bronze spring has one end attached to the coil on the inside of the bobbin and the other end fastened to a support that passes through the hole in the bobbin. The purpose of this spring is to keep the quartz fiber in tension and also to serve as a current

lead to the coil. The lucite bobbin is securely cemented to the end of a lucite piece shaped like a "T". Around the quartz fiber is another phosphor bronze spring which is the other current lead to the coil. A mirror is waxed on the "T" for the indicator.

The quartz fiber is about one hundred microns in diameter and two and one half inches long. The fiber is fused at both ends to quartz cross pieces one sixteenth of an inch in diameter and one half inch long making a long "H". The ends of these cross pieces are waxed to the "T" and to the torsion head. This makes a secure connection to the fiber.

The torsion head is used to rotate the end of the quartz fiber through a reproducible angle of about 160 degrees and thus apply the restoring torque to the coil. This is achieved by stops that limit the rotation at the torsion lever. These stops are on a plate that can be rotated a few degrees by screw adjustment. The "zero" position is set by putting the torsion lever to the "off" position and adjusting this plate until the magnetometer reads zero with no current in the coil. The torsion is then rotated to the "on" position for measuring the magnetic field.

The coil is placed in a small cup at the edge of the vacuum chamber in the fringing field of the magnet as shown in Figure 3. The fringing field measured by the magnetometer is proportional to the field at the equilibrium orbit over the entire range of the spectrometer to the accuracy that the magnetometer can measure the fringing field.

The indicator is a diamond shaped beam of light reflected off of the mirror to a 920 phototube. The lever arm of the light beam is 26 inches. The 920 has two cathodes and two anodes parallel to each other. Hence, by taking the difference of the output of the two sides of the tube one can tell which side the light beam is on.

The associated electronic equipment consists essentially of the phototube, a converter to convert the d.c. signal of the light beam to an a.c. signal, two identical feed back amplifiers in parallel and two phase detectors. The diagram is shown in Figure 4. The anodes of the phototube are connected across a centertapped transformer with the centertap grounded. Each half of the phototube conducts on every other half cycle. This develops a rather large 120 cycle signal. Superimposed on this signal is a small 60 cycle signal which is the error signal, and the phase of which depends upon which half of the phototube conducts the most, i.e., which half receives the most light. The capacitor across the imput of the preamplifier removes much of the unwanted 120 cycle signal. Because of the very high impedance of the phototube, a trimmer capacitor of 10 uuf was placed across the anode of one of the halves of the phototube.

The output of the preamplifier goes to two separate amplifiers through two separate attenuation controls. The amplifiers are identical two stage amplifiers with feed back. The phase detectors are similar. The output of one runs a balance meter and generator field resistor control, and the output of the other

controls the field of the amplidyne. If there is no signal on the 6L6 tube (see Figure 4) both 6X5's conduct the same on alternate half cycles. If there is a signal of one phase the 6L6 conducts more on one half cycle than on the other. Hence, one of the 6X5's draws more current during its half cycle than the other during the other half cycle. This gives a net current through the field of the amplidyne in one direction. If the phase is reversed then the net current through the amplidyne field is also reversed.

With this magnetometer and control circuit one can measure the magnetic field to one part in a thousand or better. The current through the magnetometer coil is measured by a potentiometer and a precision resistor. The magnetic field can be regulated to better than one part in ten thousand.

To compensate for large drifts due to heating of the coils and field resistors, an automatic field adjustor (not shown in Figure 4) has been built. This consists of a Weston meter switch, which closes contacts with as little as fifteen microamperes, placed in series with the magnetometer balance meter. By means of relays this meter switch operates a motor which varies the field resistors of the spectrometer generator. The field resistance is automatically adjusted when the magnetic fields drift as little as one part in 20,000.

PART IV

DETERMINATION OF CROSS SECTION

The determination of the cross section is possible if the solid angle of the magnetic spectrometer, its resolution, the number of incident particles and the thickness of the target are known. The number of observed counts is given by

$$N = n_o nt \Omega \frac{d\sigma}{d\Omega} \quad . \tag{8}$$

Where N is the number of counts, $d\sigma/d\Omega$ the differential cross section, Ω the solid angle of the spectrometer, n_o the number of incident particles, n the number of disintegrable nuclei per cubic centimeter, and t the thickness of the target. The quantity n_o is found by measuring the charge collected at the target by a current integrator from the equation

$$n_o = CV \times 6.24 \times 10^{12}/z \quad \text{particles per microcoulomb.} \tag{9}$$

Here C is the capacitance of the current integrator and V the firing voltage of the current integrator, while ze is the charge on the particles.

For a thin target, nt is the number of disintegrable nuclei per square centimeter. This can be determined for a thin lamina in a thick target from

$$nt = \xi_1/\varepsilon_1 = \frac{\text{Energy loss of protons in target lamina}}{\text{Stopping cross section of target nuclei}} \quad . \tag{10}$$

To find ξ_1/ε_1, note from Figure 5 that

$$\Delta E_1 = \xi_1 = \frac{xn\varepsilon_1}{\cos \theta_1} \qquad \text{or} \qquad xn = \frac{\xi_1 \cos \theta_1}{\varepsilon_1} \tag{11}$$

and

$$\Delta E_2 = \xi_2 = \frac{xn\varepsilon_2}{\cos \theta_2} \qquad \text{or} \qquad xn = \frac{\xi_2 \cos \theta_2}{\varepsilon_2} \tag{12}$$

where the subscript designates the particle before and just after it is scattered. Now the total energy spread of the outgoing particle is given by

$$\delta E_2 = \frac{\partial E_2}{\partial E_1} \xi_1 + \xi_2 \tag{13}$$

where

$$\frac{\partial E_2}{\partial E_1} = \alpha = \left| \frac{M_1 \cos \theta}{M_1 + M_2} \pm \frac{(M_2^2 - M_1^2 \sin^2 \theta)^{1/2}}{M_1 + M_2} \right|^2 . \tag{14}$$

Here M_1 is the mass of the bombarding particle, M_2 the mass of the target nuclei, and θ the scattering angle. Solving equations (11) and (12) for ξ_2 we have

$$\xi_2 = \frac{\xi_1 \cos \theta_1 \, \varepsilon_2}{\cos \theta_2 \, \varepsilon_1} \tag{15}$$

and substituting into equation (13) we obtain

$$\delta E_2 = \alpha \xi_1 + \xi_1 \frac{\cos \theta_1 \, \varepsilon_2}{\cos \theta_1 \, \varepsilon_1} \tag{16}$$

or

$$\frac{\xi_1}{\varepsilon_1} = \frac{\delta E_2}{\alpha \varepsilon_1 + \varepsilon_2 \frac{\cos \theta_1}{\cos \theta_2}} \, . \tag{17}$$

For near relativistic particles

$$P_2^2 \doteq 2E_2 M_1 \left(1 + \frac{E_2}{2M_1 c^2} \right) \, . \tag{18}$$

Differentiating, we have

$$2P_2 \delta P_2 \doteq 2M_1 \left(1 + \frac{E_2}{2M_1 c^2} \right) \delta E_2 + \frac{2M_1 E_2 \delta E_2}{2M_1 c^2} \tag{19}$$

$$= 2M_1 \left(1 + \frac{E_2}{M_1 c^2} \right) \delta E_2 \, .$$

Hence

$$\delta E_2 \doteq \frac{P_2 \delta P_2}{M_1 \left(1 + \frac{E_2}{M_1 c^2} \right)} = \frac{\delta P_2 2E_2 M_1 \left(1 + \frac{E_2}{2M_1 c^2} \right)}{P_2 M_1 \left(1 + \frac{E_2}{M_1 c^2} \right)}$$

$$= \frac{\delta P_2}{P_2} \, 2E_2 \left(1 - \frac{E_2}{2M_1 c^2} \right) \, . \tag{20}$$

Now $P_2/\delta P_2$ is the resolution R of the spectrometer, therefore

$$\delta E_2 \doteq \frac{2E_2}{R}\left(1 - \frac{E_2}{2M_1c^2}\right) \qquad (21)$$

$$= \frac{2E_2}{R} \qquad \text{non-relativistically.}$$

Substituting this into equation (17) we obtain

$$\frac{\xi_1}{\varepsilon_1} = \frac{2E_2(1 - E_2/2M_1c^2)}{R\left(a\varepsilon_1 + \varepsilon_2 \frac{\cos\theta_1}{\cos\theta_2}\right)} . \qquad (22)$$

The resolution is given by

$$R = 2(1 + M)r_o/\delta r \ ^{*}. \qquad (23)$$

Where M is the magnification of the spectrometer and r_o the radius of the equilibrium orbit. In the spectrometer employed in this experiment r_o is 10.5 inches. The quantity δr is the width of the exit slit employed. There are four exit slits of varying sizes that could be used. Thus R equals 37.8 inches/δr. Thus making the appropriate substitutions we get for the differential cross section

$$\frac{d\sigma}{d\Omega} = \frac{N\left(a\varepsilon_1 + \varepsilon_2 \frac{\cos\theta_1}{\cos\theta_2}\right) 37.8 \left(1 + \frac{E_2}{2M_1c^2}\right) Mc \text{ in}}{\Omega CV\ \delta r\ 6.24 \times 10^{-12} \text{ protons } 2E_2} . \qquad (24)$$

---

* This is equation (8) page 861, Snyder et al. (2) with n = 1/2.

The term $E_2/2M_1c^2$ is the relativistic correction. As stated before, this correction is at most 0.1 per cent for protons of energies less than two mev.

There are three different apertures that one may use on the spectrometer that define the solid angle. The efficiency of the counter has been incorporated into the calculated effective solid angle for each aperture.

The target angle is always set so that $\theta_1 = \theta_2$, thus if C is in microfarads, V in volts, δr in inches, E_2 in kev, ε_1 and ε_2 in ev cm^2, and Ω in steradians, the differential cross section is in the laboratory system

$$\frac{d\sigma}{d\Omega} = \frac{N(a\varepsilon_1 + \varepsilon_2)\ 3.03 \times 10^{-12}\ cm^2}{\Omega CV\ \delta r\ \ E_2} \quad . \tag{25}$$

To obtain the cross section in the center of mass system we must use the formula

$$\frac{d\sigma_{cm}}{d\Omega} = \frac{(1 + \gamma \cos\theta)^{d\sigma_{LAB}/d\Omega}}{(1 + \gamma^2 + 2\gamma \cos\theta)^{3/2}} \tag{26}$$

Where θ is the center of mass angle and γ is M_1/M_2.

The only quantity not directly measured in equation 25 is the stopping cross section ε. The stopping cross section used in these calculations was that calculated by Hirshfelder and Magee [6]. Reynolds, Whaling and Wenzel[7,8] have measured the stopping cross section for carbon up to 600 kev. Their values are

about seven to eight per cent lower than Hershfelder and Magee's. If one uses Bethe's formula[9] and Segre's value for the average ionization potential of carbon I = 74.4 ev [10], and calculates the stopping cross section he agrees with the values of Reynolds, Whaling, and Wenzel (see Table 1).

Whaling and Wenzel[11] have also measured the stopping cross section for copper and found that the values given by Warshaw[12] are 6 per cent high. The efficiency of the counter was calculated by scattering protons from copper and assuming that the scattering obeys the Rutherford scattering law. Warshaw's stopping cross section for copper was used in the calculations. This means that the efficiency of the counter calculated was too high by 6 per cent and the calculated cross section of carbon was too low by 6 per cent. However, this error just about balanced the error of the stopping cross section of the carbon that was used. The one of two per cent error remaining is of the order of the experimental errors and, hence, the data has not been recalculated using the newer values of the stopping cross section and counter efficiency.

TABLE 1

COMPARISON OF THE STOPPING CROSS SECTION FOR CARBON.

E_p	Hirshfelder and Magee	Reynolds Whaling Wenzel	Calculated	Per cent Difference
Kev	ev cm^2 x 10^{15}			
300	11.09	10.20		8.0
400	9.28	8.54		8.0
500	8.00	7.38		7.7
600	7.09	6.55	6.55	7.6
1,600	3.56		3.32	6.8

PART V

TARGETS

If at a given bombarding energy the number of scattered particles (counts) is plotted against the magnetometer setting, a curve known as a profile is obtained. These curves (examples are shown in Figures 6, 7) give a good indication of the condition of the target surface. If there are contaminations of heavier elements on the surface of the target they will show up as peaks in front of the front edge of the target. The front edge will slope off instead of being sharp if the surface is too rough and if there are contaminations on the surface. The surface contaminants can be determined by the momentum of the scattered particles by using equation (11). The particles at the frontedge are scattered from the surface of the target. Those further from the front are scattered from deeper layers. Because of straggling which will smear out the peaks and dips of the resonances it is advisable to operate near the front of the profile. This is especially true if the resonance is very sharp.

The surface contaminants are usually just carbon and oxygen which arise from the pump oil that is present in the vacuum system. Other contaminants usually arise from improper handling of the targets outside the target chamber. The accumulation of oxygen on the surface is especially bad if the target readily reacts with oxygen or water. The oxygen and carbon contaminants

can be kept down to a minimum if there is good cold trapping in the target vacuum system. The carbon contaminants can be kept down by heating the target to about 130 degrees centigrade. However, if the target material readily reacts with oxygen then the oxygen build up on the surface is much greater if the target is heated. In the case of carbon targets, however, the heating reduced the accumulation of oxygen. The carbon build up was, of course, no problem in the case of C^{12} targets. It was necessary to heat the C^{13} targets to keep the C^{12} from depositing on the surface. The carbon and oxygen accumulate on the bombarding spot. Therefore, if the target can be moved so that the beam hits several different spots, then the same target can be used longer before it has to be replaced.

Several types of carbon targets were made and used. The easiest type to make is the soot target. A copper blank is held in the smoky flame of burning benzine until there is a thick uniform layer of lampblack on the target. These targets stood up under continued bombardment. The targets were very good for large scattering angles. Because of the very granular and porous structure of lampblack the profiles were not very sharp, especially for the small scattering angles, hence they were not very good for the small scattering angles.

For C^{13} targets soot is unsatisfactory, since it is very wasteful of the C^{13}. The C^{13} is obtained from Eastman Kodak Company in the form of methyl iodide. It is 61 per cent C^{13} and 39 per cent C^{12}.

Dr. John Seagrave[13] developed a method of making targets by cracking methane or methyl iodide on a very hot tantalum strip. He used this method for making thin carbon targets that did not peel off. This type is good for scattering experiments at small scattering angles and low energies. The thick targets would always blister off of the tantalum strip when the strip was cooled. Thick carbon foils were made in this manner.

The procedure used was slightly different than that used by Dr. Seagrave to make C^{12} targets. About one half atmosphere of methane was introduced into the cracking chamber after the cracking chamber had been evacuated and the tantalum strip heated to a bright yellow by passing an electric current through it. The cracking chamber is shown in Figure 8. The cracking proceeded rapidly and after a few seconds the waste hydrogen from the cracking process was pumped out and more methane introduced. This was repeated about four times depending upon how thick the targets were desired. The last time the waste hydrogen was not pumped out. This helped to prevent the foil from shattering when it blisters. The current was then turned off slowly and the tantalum strip removed from the cracking chamber. Usually a large blister formed when the strip was cooled. The carbon foil was then carefully removed from the strip. One can obtain foils 1 x 3 cm. in this manner. If the foil was too thin it would not blister. Some of the thin foils could be made to blister by dipping them in

liquid nitrogen. It would be desirable to have the thick foils stick to the tantalum and not blister, but because of the different coefficients of thermal expansion the thick layers always blistered off.

To make C^{13} targets, the following procedure was used. The C^{13} enriched methyl iodide is first frozen by placing the container in liquid nitrogen. Then the container is pumped out to remove the air and sealed off by means of a pinch clamp. A thick layer of C^{12} was cracked on the tantalum strip from methane and all of the waste hydrogen pumped out. One sixth of an atmosphere of the C^{13} enriched methyl iodide vapor was introduced into the cracking chamber. The vapor transfer system is shown in Figure 9. The methyl iodide decomposed much more easily than methane, and, hence, was completely cracked in a few seconds. The waste hydrogen and iodine was then pumped out. This was repeated twice. The last time the waste hydrogen and iodine had to be pumped out or the iodine would deposit on the carbon when the tantalum was cooled. This method produces a thick target of low atomic weight and yet conserves the C^{13}.

If the target backing is some material of high atomic weight, then the target material must be thick enough so that the protons scattered off of the backing material lose more energy in passing through the layer of target material than the protons lose in being scattered by the target nuclei. The necessary

thickness is given by

$$2t > (\alpha_1 - \alpha_2)\, E_b/\sin \theta/2 \qquad (27)$$

Where t is the thickness of the target in energy loss of the protons passing through it, $\alpha_1 = E_2/E_1$ of the backing material, and $\alpha_2 = E_2/E_1$ of the target nuclei and θ is the scattering angle. For small scattering angles and low energies thin unblistered targets could be used. For the large scattering angles the blistered targets were used.

The blistered foils were pasted on to the copper blanks by either saliva or vacuum grease. The saliva was very good if it was allowed to dry thoroughly before being placed in the vacuum. The vacuum grease was better if it was desired to put the target in the vacuum system immediately. However, the foil would wrinkle and buckle under bombardment if the vacuum grease was used.

The foils have a very smooth surface and, hence, give a very sharp profile. Hence, they were very good for sharp resonances because the sharp profile allowed one to work in a lamina nearer to the surface of the target. The nonblistered targets are best for the small scattering angles because they do not wrinkle. The best foil targets eventually warp and buckle under bombardment.

PART VI

EXPERIMENTAL PROCEDURE

Before running the machine several calculations had to be made. First the laboratory scattering angle θ_L was calculated from the formula

$$\tan \theta_L = \sin \theta/(\gamma + \cos \theta) \qquad (28)$$

where θ is the center of mass scattering angle and γ is M_1/M_2. Then the quantity α was calculated from equation (14) for each scattering angle.

A profile was then made of a target to determine whether is was a suitable target for the angle to be studied. If it was not suitable another target was tried. If the profile was sharp with no contaminations on the surface, then a point near the top of the curve just behind the front edge was chosen. The so called following constant for the particular angle was calculated from this point from the formula $E_p I^2 = K$. The following constant K can be calculated from the spectrometer constant k_p, the electrostatic analyzer constant C and the per cent energy loss in the target. For

$$E_1 = E_b - \Delta E_1$$

where E_b is the bombarding energy and ΔE_1 the energy loss of the proton in the target before being scattered.

$$E_b = CE_p$$

and E_p is the setting of the electrostatic analyzer. The energy of the particles counted by the spectrometer E_{20} is then given by

$$E_{20} = \alpha E_1 - \Delta E_2 = \alpha C E_p - \Delta E_2 - \alpha \Delta E_1 = k_p / I^2$$

or solving for $E_p I^2$ we have

$$E_p I^2 = k_p/\alpha C + \alpha \Delta E_1 I^2/\alpha C - \Delta E_2 I^2/\alpha C$$

$$= \frac{k_p}{\alpha C}\left(1 + \frac{E}{E_{20}}\right) = K \qquad (29)$$

where δE is the energy loss in the target. From this formula the value for I was determined for each bombarding voltage.

Data for elastic scattering of protons by C^{12} was taken at every ten degrees in the center of mass system from 30 to 160 degrees in the energy range from 300 to 600 kev. The following constants were calculated for a 1 per cent energy loss in the target. Two persons were necessary to operate the machine. One person operated the Van de Graaff generator and electrostatic analyzer and the other operated the magnetic spectrometer and recorded the data. The data from 400 to 600 kev

was taken using the mass I beam and the data from 300 to 450 was taken using the mass II beam*.

The ratio of the observed cross section to Rutherford cross section for carbon twelve is plotted for the various angles in Figures 9 - 13.

Since the C^{13} targets were not pure C^{13}, but 61 per cent C^{13} and 39 per cent C^{12} the procedure was different. The profiles for C^{13} are shown in Figures 6 and 7. It was possible to separate the protons scattered from C^{13} from those scattered from C^{12} at angles larger than 100 degrees. The scattered protons from C^{12} have less energy than those scattered from C^{13} because of the different masses. For angles greater than 100 degrees the following constant was chosen so that the protons from C^{13} were counted but not those scattered from C^{12}. For angles less than 100 degrees the separation of the scattered protons from the two isotopes was of the order of the resolution of the spectrometer or less and hence, they could not be separated. For the small scattering angles, both C^{12} and C^{13} targets were placed on the target blank. A point

---

* The proton beam consists of three components H^+, HH^+, and HHH^+ designated as mass I, II, and III respectively. They are separated by a magnetic cross field between the electrostatic generator and the electrostatic analyzer. The protons in the mass II beam have half the energy of those in the mass I, while those in the mass III have one third the energy. Thus for scattering experiments at low energies where the machine would be unsteady the mass II or III beam is used.

was taken with each target at each energy. The yield for the pure C^{13} is then given by

$$N = \frac{(N_{C^{13}} - 0.39N_{C^{12}})}{0.61} \qquad (30)$$

where $N_{C^{13}}$ is the number of counts from the impure C^{13} target and $N_{C^{12}}$ is the number of counts from the C^{12} target. The quantity $0.39N_{C^{12}}$ was plotted and a smooth curve was drawn through the points. The values for the above formula were taken from this curve.

Except at a few points at the dips of the resonances, over 10,000 counts were taken at each point. Thus the statistical uncertainity given by the coefficient of variation $\pm \sqrt{N}/N$ of the number of counts N was less than 1 per cent in most cases. The coefficient of variation is the standard deviation $\pm \sqrt{N}$ divided by the number of counts N. The least number of counts taken at any point is of the order of 2500 counts giving a maximum coefficient of variation of 2 per cent for the C^{12} and C^{13} at large angles.

The standard deviation for the sum or difference of two numbers is the square root of the sum of the squares of the standard deviations. Hence, the coefficient of variation for the scattering at small scattering angles of C^{13} is quite large. For example, for $N_{C^{13}} = 18{,}000$ counts and $N_{C^{12}} = 19{,}000$ counts the coefficient of variation is still 1.5 per cent. The coefficient of variation for the small angle

scattering of C^{13} was about 1.5 - 4 per cent. The irregularities of the target surface which are troublesome at small angles limited the accuracy to about 5 - 10 per cent at the small scattering angles.

The number of counts read from the counters must be corrected for the resolving time of the counter; and if a small capacitor is used in the current integrator for a long running time the counts must be corrected for current integrator leakage.

The data for C^{13}(pp) C^{13} is shown in Figures 15 - 22.

PART VII

ANALYSIS OF $C^{12}(pp)C^{12}$

In order to determine the nature of the levels that give rise to these resonances it is necessary to fit the partial wave expansion of the differential cross section for the elastic scattering of the protons to the data. For target nuclei with zero spin this expansion is[14]

$$d\sigma/d\Omega = \eta/k^2 \Big| - 1/2 \csc^2 \theta/2 \exp(i\eta \ln \csc^2 \theta/2)$$
$$+ \sum_{\ell=0}^{\infty} [(\ell + 1) \sin \delta_\ell^+ \exp(i\delta_\ell^+)$$
$$+ \ell \sin \delta_\ell^- \exp(i\delta_\ell^-)] P_\ell(u) \exp i\alpha_\ell \Big|^2$$
$$+ \frac{\sin^2 \theta}{k^2} \Big| \sum_{\ell=1}^{\infty} (\sin \delta_\ell^+ \exp(i\delta_\ell^+)$$
$$- \sin \delta_\ell^- \exp(i\delta_\ell^-)) P_\ell'(u) \exp i\alpha_\ell \Big|^2 \quad * \qquad (31)$$

where $u = \cos\theta$, $d\sigma/d\Omega$ is the differential cross section in the center of mass system, $k = 1/\chi = uv/\hbar$, $u = \frac{M_1 M_2}{M_1 + M_2}$ = reduced mass, $\eta = \frac{ZZ'e^2}{\hbar v}$, $\delta_\ell^{\pm}$ is the non-coulomb phase shift and

$$e^{i\alpha_\ell} = \prod_{s=1}^{\ell} \left(\frac{s + i\eta}{s - i\eta} \right) \qquad \text{for} \qquad \ell > 0$$

and $e^{i\alpha_0} = 1$

---

* This follows from equations 4 and 5, C.L. Critchfield and D.C. Dodder, Phys. Rev. 76, 602 (1949).

The first squared bracket is the coherent scattering term, i.e., the scattering of those protons whose spins do not change direction and the second, the incoherent part the scattering of the protons whose spins do change direction. The first term in the first bracket is the coulomb scattering term. The assumptions in this formula are: 1 the elastic scattering is by far the most probable process, and 2 the observed scattering anomalies involve only one level of a given angular momentum, i.e., one level formula. The only other process taking place in competition with the elastic scattering from C^{12} is radiative capture. The elastic scattering is by far the most probable and the radiative capture can be neglected. Jackson and Galonsky[15,16] have performed a complete analysis of the data at Wisconsin[17,18]. An analysis has been carried out on the data obtained here. The results agree with those obtained at Wisconsin.

It was first assumed that the anomaly at 460 kev. in the scattering from C^{12} is caused by just one single level in N^{13}. Under this assumption and a glance at the data at 90 degrees shows that the level cannot be formed by p-wave protons ($\ell = 1$) since $P_1(\cos 90') = 0$ in the coherent scattering term and the incoherent scattering term can only increase the cross section at resonance. Levels formed by higher angular momentum are ruled out because of Wigner's Criterion[19]. This leaves s-wave $J = 1/2^+$. The rest of the analysis is on the assumption that the level is $J = 1/2^+$ in N^{13}

$$\delta_\ell^{\pm} = \tan^{-1} \frac{F_\ell}{G_\ell} \approx 0 \quad \text{at this energy for} \quad \ell \geq 1$$

$\tan^{-1} \frac{F_\ell}{G_\ell}$ is tabulated[20]

$$\therefore \quad \frac{d\sigma}{d\Omega} \quad \text{reduces to}$$

$$\frac{1}{k^2} \left| - \frac{\eta}{2} \csc^2 \frac{\theta}{2} \exp \left[i \eta \ln \csc^2 \frac{\theta}{2} \right] \right. \tag{32}$$

$$\left. + \sin \delta_o \exp i \delta_o \right|^2$$

or

$$\frac{\sigma}{\sigma_r} = \left| - \exp\left[i \eta \ln \csc^2 \frac{\theta}{2} \right] \right. \tag{33}$$

$$\left. + \frac{2 \sin^2 \theta/2}{\eta} \sin \delta_o \exp i \delta_o \right|^2 .$$

The quantity δ_o was calculated using this formula and the angular distribution of the elastic scattering. The phase shift δ_o is plotted in Figure 23.

PART VIII

ANALYSIS OF $C^{13}(pp)C^{13}$

Dr. John Seagrave[13] has investigated the yield for the $C^{13}(p\gamma)N^{14}$ reaction from 400 kev - 2.5 mev. He observed resonances at 0.55, 1.16, 1.25, 1.76, and 2.1 mev. He also observed two small peaks in his yield curve at 1.47 and 1.55 mev, but because of the low intensity of these two resonances he could not definitely attribute them to $C^{13}(p\gamma)N^{14}$. He supposed that they might be caused by impurities in the target, but he was not able to find any light nuclei that had sharp resonances at these energies. The scattering data shows plainly that these are resonances in $C^{13}(pp)C^{13}$. The scattering shows resonances at 0.55, 1.16, 1.47, and 1.55. The broad resonance at 1.25 does not show up explicitly in the scattering, and the 1.76 and 2.1 mev resonances were not studied.

Seagrave assumed from his gamma ray experiments that the 8.07 mev level in N^{14} is formed by s-wave protons. The scattering experiments agree with this assumption. The possibility that it might be p-wave is thrown out because of the dip in the scattering at 90 degrees. The proton has a spin of $1/2^+$ and C^{13} has a spin of $1/2^-$; thus the state in N^{14} can be either $J = 0$ or 1^-. The ratio of maximum to minimum of the scattering agrees with the assignment of $J = 1^-$; the ratio is too large for $J = 0^-$.

The broad 8.70 level in N^{14} is also formed by s-wave protons at 1.25 mev. This scattering is not observed in the scattering explicitly. Mr. Gerald Speisman has been calculating the s-wave phase shifts in the neighborhood of this resonance and has found that the J = 0 s-wave phase shift could be going through a resonance. This level has therefore been assigned $J = 0^-$.

The data for the 1.16 mev resonance is rather poor because the resonance is so sharp. Dr. R.F. Christy has tried to fit the data with various assignments for the 8.62 level in N^{14}. He obtained a reasonable fit for p-wave protons and J = 0 and 1^+. Mr. Hugh Woodbury from his capture gamma ray experiments reports a transition to the 2.31 mev level in N^{14} which is known to be $J = 0^+$. If this is true then J = 0 is excluded since 0 - 0 transitions are forbidden. Until better data is obtained on this resonance the best assignment is $J = 1^+$.

No complete analysis has been performed on the 1.465 or 1.550 mev resonances. Because there is a dip in the scattering at 90 degrees, the 8.90 level in N^{14} is formed by either s, d, or g-wave protons at 1.465 mev. Wigner's criterion eliminates the possibility of g-wave and the complexity of the scattering at the various angles rules out s-wave. The assignment of this level is $J = 2$ or 3^-. The assignment $J = 1^-$ is excluded because the level could then be formed by s-wave protons.

The 8.98 mev level in N^{14} is probably formed by p-wave protons at 1.550 mev. The scattering has a symmetrical peak at ninety degrees. This would indicate p or f-wave protons. The f-wave is excluded by the Wigner criterion. Until the data is analyzed the assignment stands at $J = 0, 1$ or 2^{+}.

REFERENCES

(1) Fowler, Lauritsen, and Lauritsen, Rev. Sci. Inst., 18, 818 (1947).

(2) Snyder, Rubin, Fowler, and Lauritsen, Rev., Sci. Inst., 21, 852 (1950).

(3) Warters, W.D., Ph. D. Thesis, California Institute of Technology, (1953).

(4) Lauritsen, C.C. and T. Lauritsen, Rev. Sci. Inst., 19, 916 (1948).

(5) Strong, J., Procedures in Experimental Physics, Prentice Hall, pp. 188-216 (1938).

(6) Hirshfelder, J. and Magee, J., Phys. Rev., 73, 207 (1948).

(7) Reynolds, H.K., Ph. D. Thesis, California Institute of Technology, (1953).

(8) Reynolds, H.K., D.N.F. Dunbar, W.A. Wenzel, and W. Whaling, Phys. Rev. (in press).

(9) Livingston, M. Stanley, and H.A. Bethe, Rev. Mod. Phys. 9, 264 (1937).

(10) Mather, R. and Segrè, E., Phys. Rev., 84, 191 (1951).

(11) Whaling, W. and W.A. Wenzel, private communication.

REFERENCES

(12) Warshaw, S.D., Phys. Rev., 76, 1759 (1949).

(13) Seagrave, John, Phys. Rev., 85, 197 (1952).

(14) Critchfield, C.L. and D.C.Dodder, Phys. Rev., 76, 602 (1949).

(15) Jackson, H.L. and A.I. Galonsky, Phys. Rev., 84, 401 (1951).

(16) Jackson, H.L. and A.I. Galonsky, Phys. Rev., 89, 370 (1953).

(17) Goldhaber, G. and R.M. Williamsen, Phys. Rev., 82, 495 (1951).

(18) Jackson, Galonsky, Eppling, Hill, Goldberg and Cameron, Phys. Rev., 89, 365 (1953).

(19) Wigner, E.P. and L. Eisenbud, Phys. Rev., 72, 29 (1947).

(20) Block, Hull, Jr., Broyles, Bouricius, Freeman, and Breit, Rev. Mod. Phys., 23, 147 (1951).

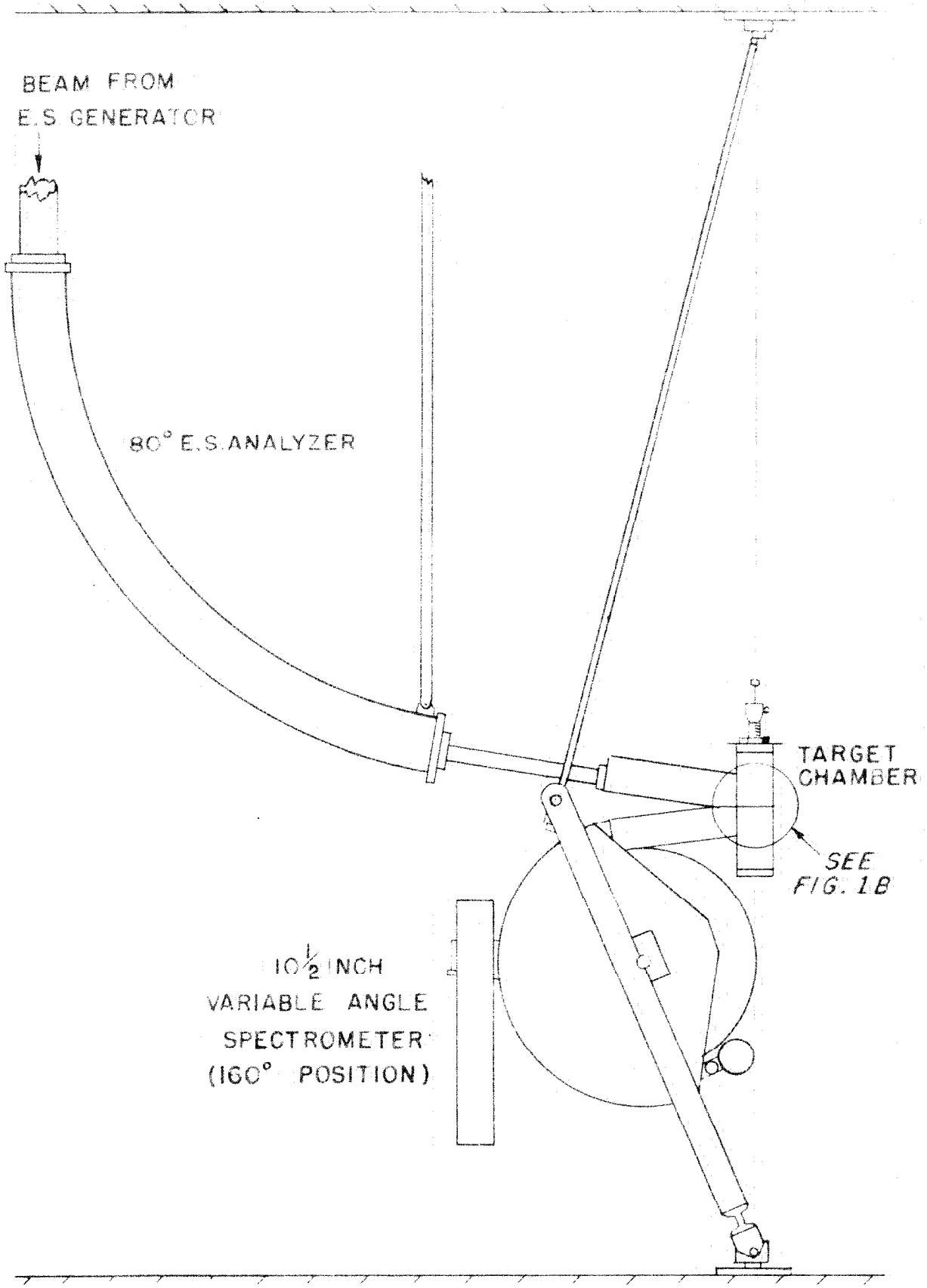

FIGURE 1A - LAYOUT OF APPARATUS

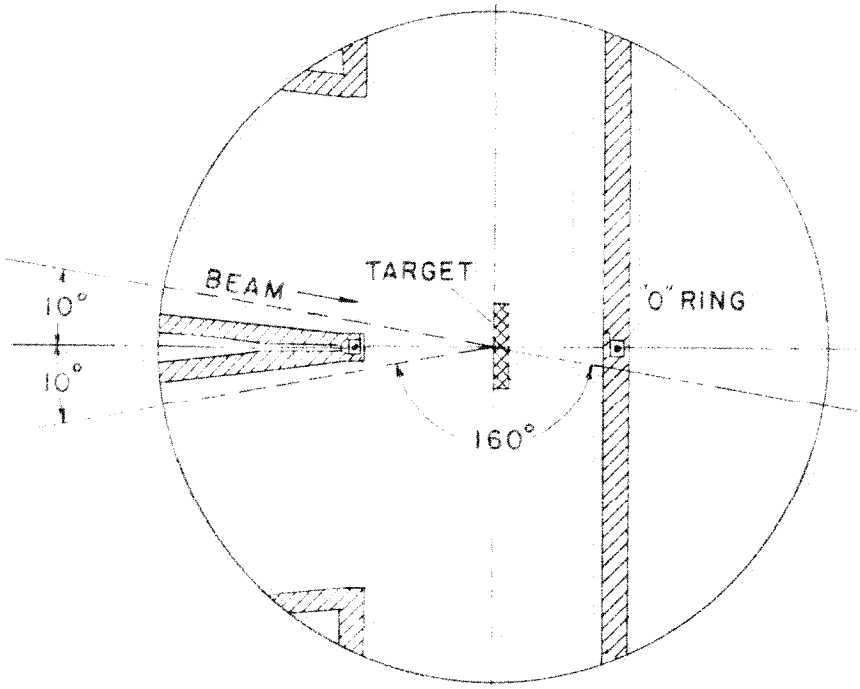

160° POSITION

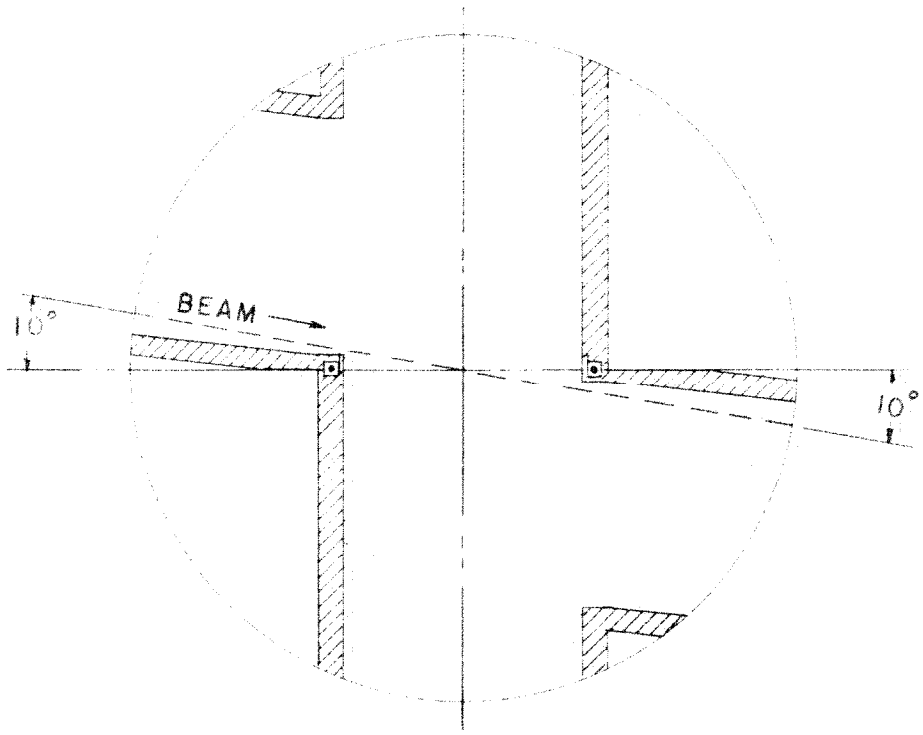

0° POSITION

FIGURE 1B - TARGET CHAMBER DETAIL

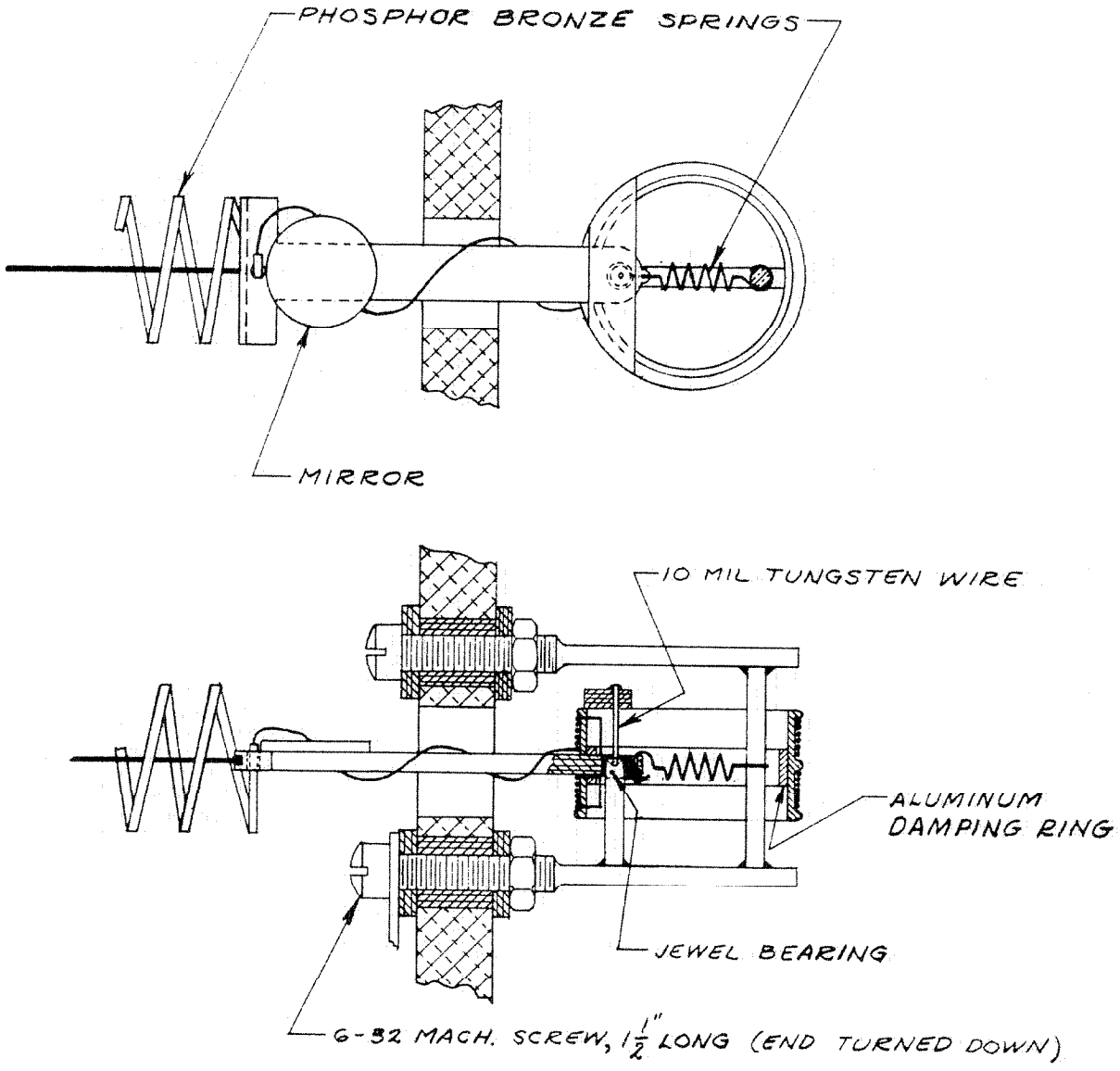
PHOSPHOR BRONZE SPRINGS
MIRROR
10 MIL TUNGSTEN WIRE
ALUMINUM DAMPING RING
JEWEL BEARING
6-32 MACH. SCREW, 1 1/2" LONG (END TURNED DOWN)

FIGURE 2

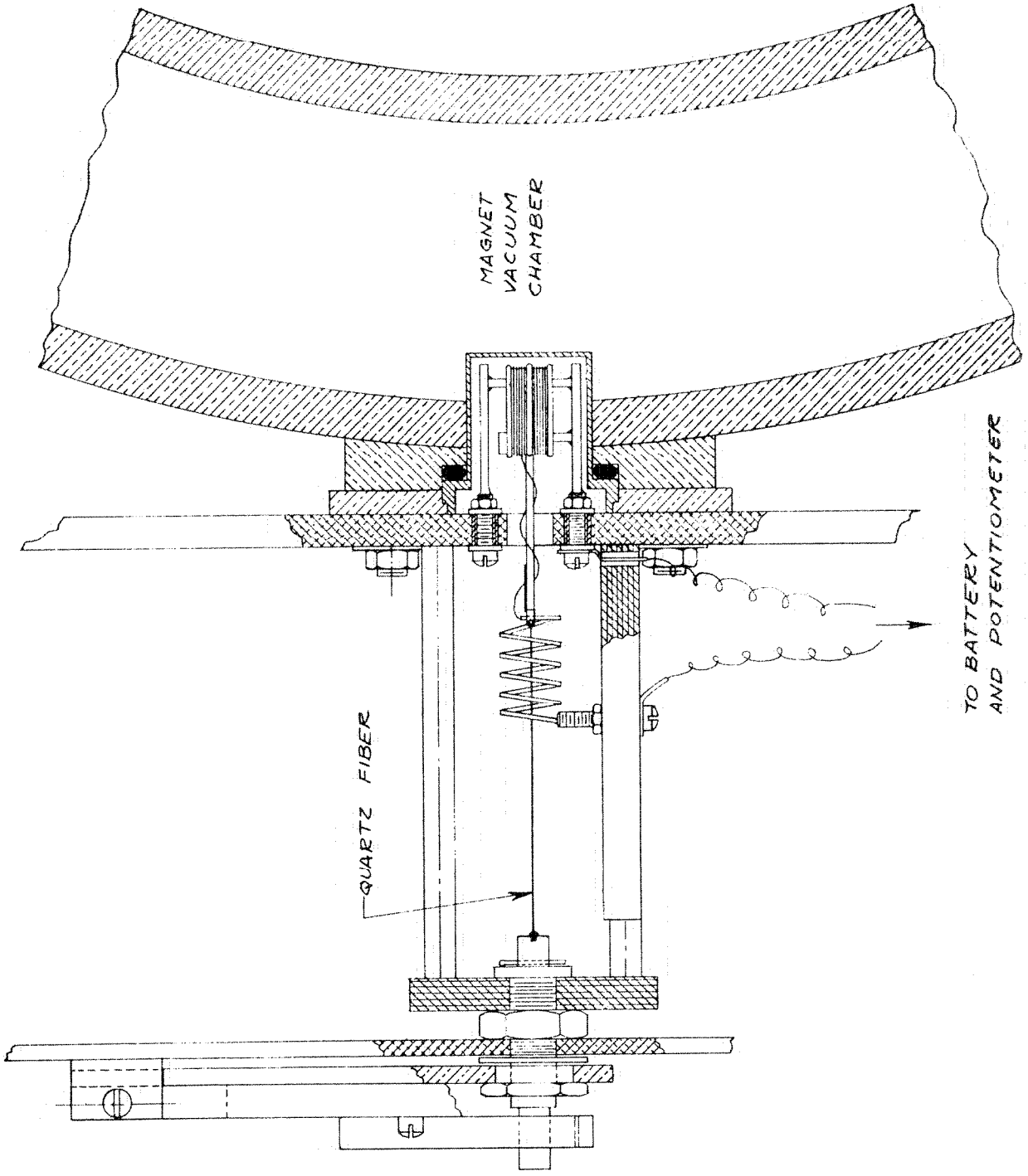
MAGNET
VACUUM
CHAMBER
TO BATTERY
AND POTENTIOMETER
QUARTZ FIBER

FIGURE 3

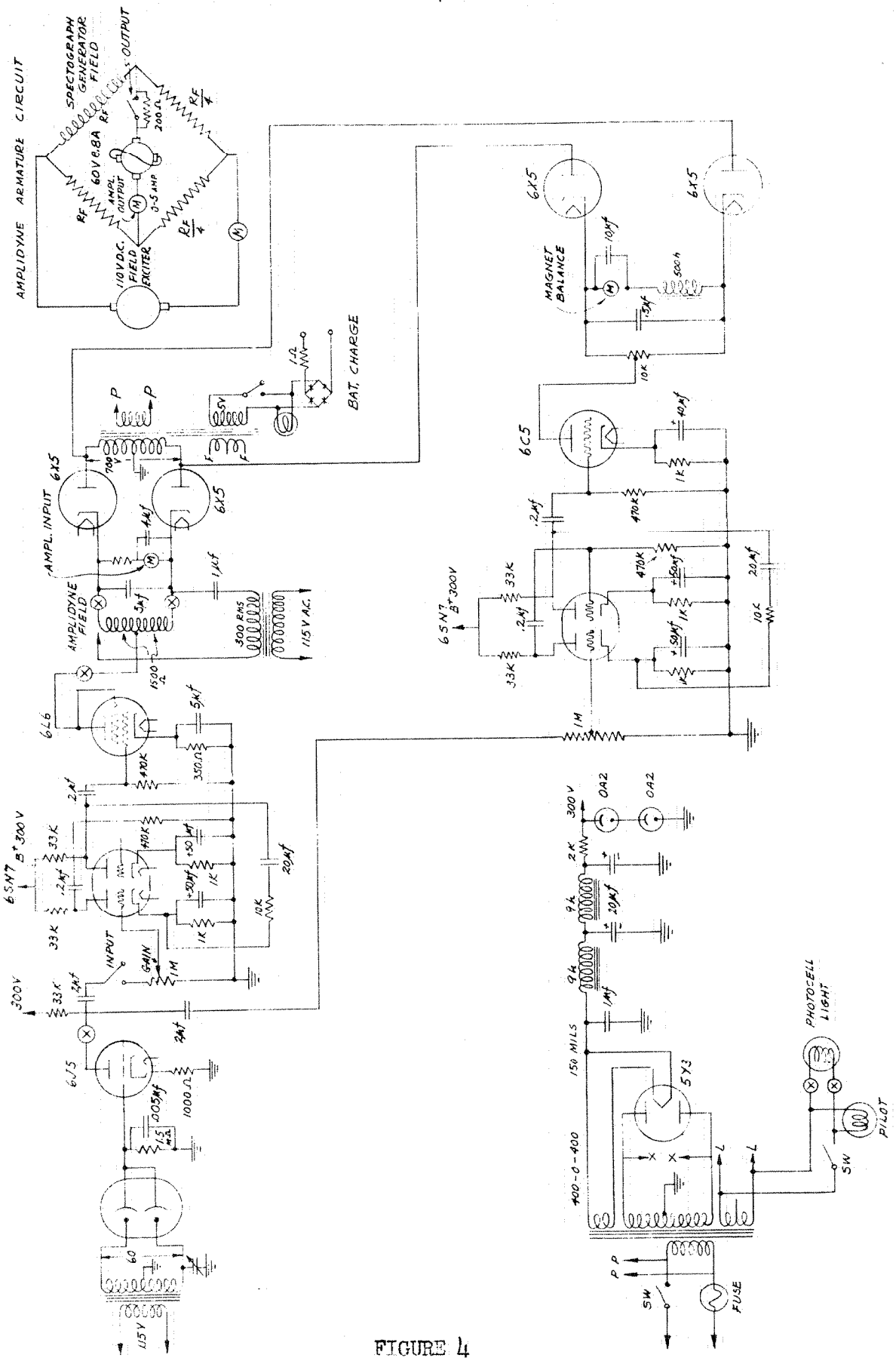
AMPLIDYNE ARMATURE CIRCUIT
SPECTOGRAPH GENERATOR FIELD
60V 6.8A
RF OUTPUT
200Ω
RF/4
AMPL OUTPUT
0-5 AMP
110 V D.C. FIELD EXCITER
BAT. CHARGE
AMPL. INPUT
6X5
6C5
6J5
6L6
6SN7
AMPLIDYNE FIELD
115 V A.C.
MAGNET BALANCE
INPUT
GAIN
0A2
5Y3
PHOTOCELL LIGHT
PILOT
FUSE
SW

FIGURE 4

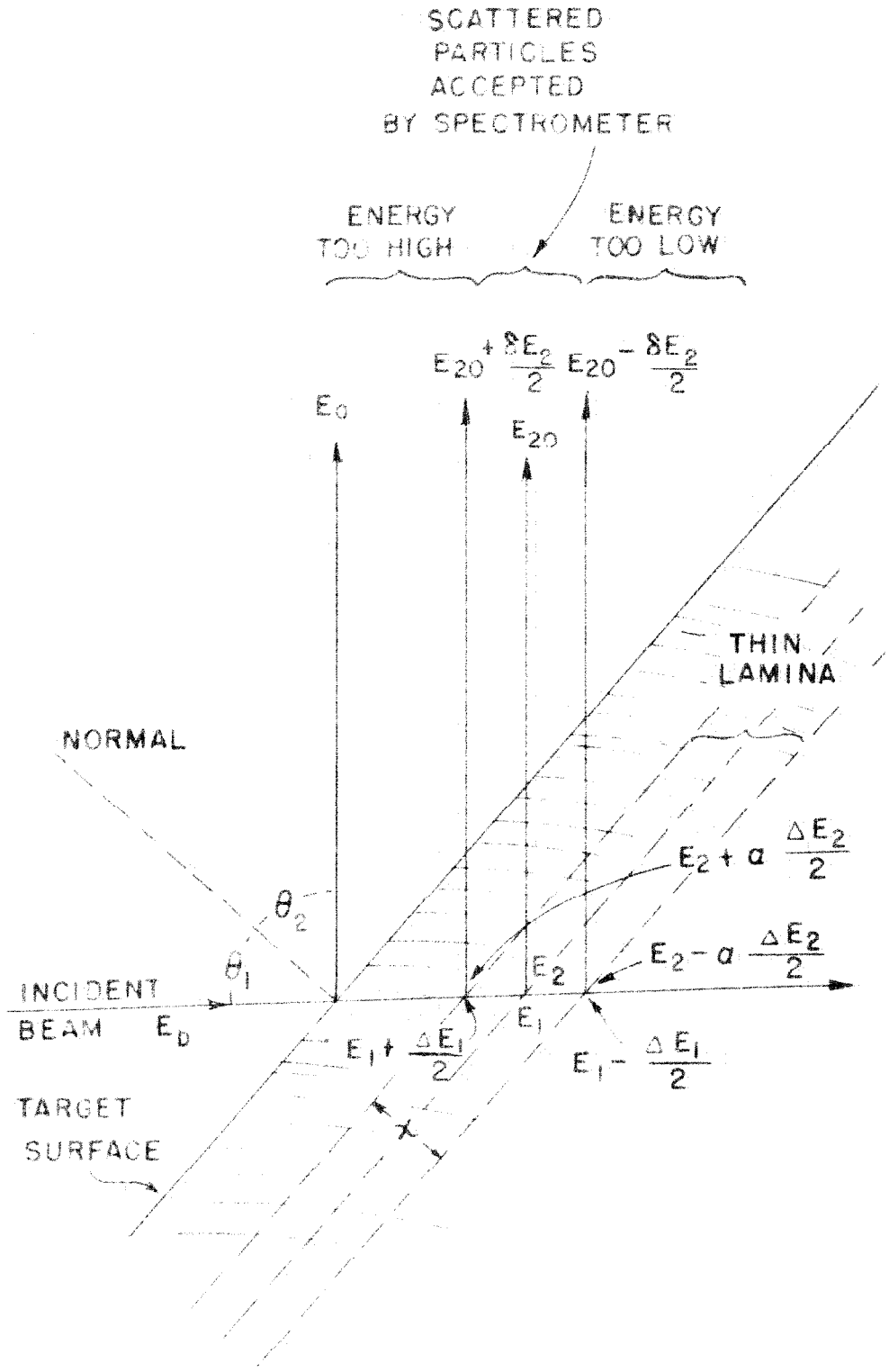
SCATTERED
PARTICLES
ACCEPTED
BY SPECTROMETER
ENERGY
TOO HIGH
ENERGY
TOO LOW
$E_{20} + \frac{\delta E_2}{2}$
$E_{20} - \frac{\delta E_2}{2}$
E_0
E_{20}
THIN
LAMINA
NORMAL
$E_2 + a \frac{\Delta E_2}{2}$
θ_2
θ_1
E_2
$E_2 - a \frac{\Delta E_2}{2}$
INCIDENT
BEAM E_0
E_1
$E_1 + \frac{\Delta E_1}{2}$
$E_1 - \frac{\Delta E_1}{2}$
TARGET
SURFACE
x

FIGURE 5

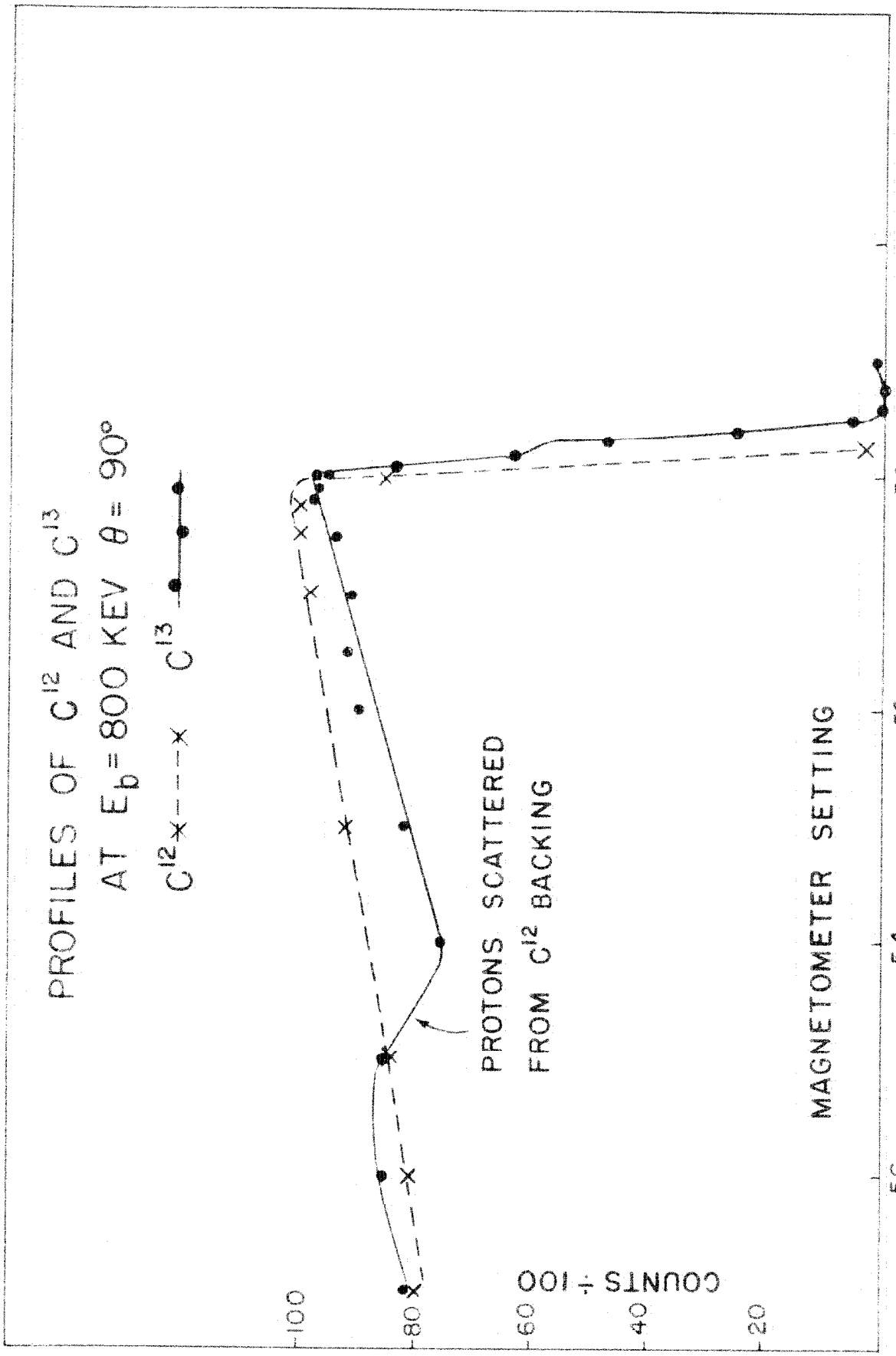
PROFILES OF C12 AND C13
AT Eb = 800 KEV θ = 90°
C12 × - - - × C13
PROTONS SCATTERED
FROM C12 BACKING
MAGNETOMETER SETTING
COUNTS ÷ 100
100
80
60
40
20
48
50
52
54
56

FIGURE 6

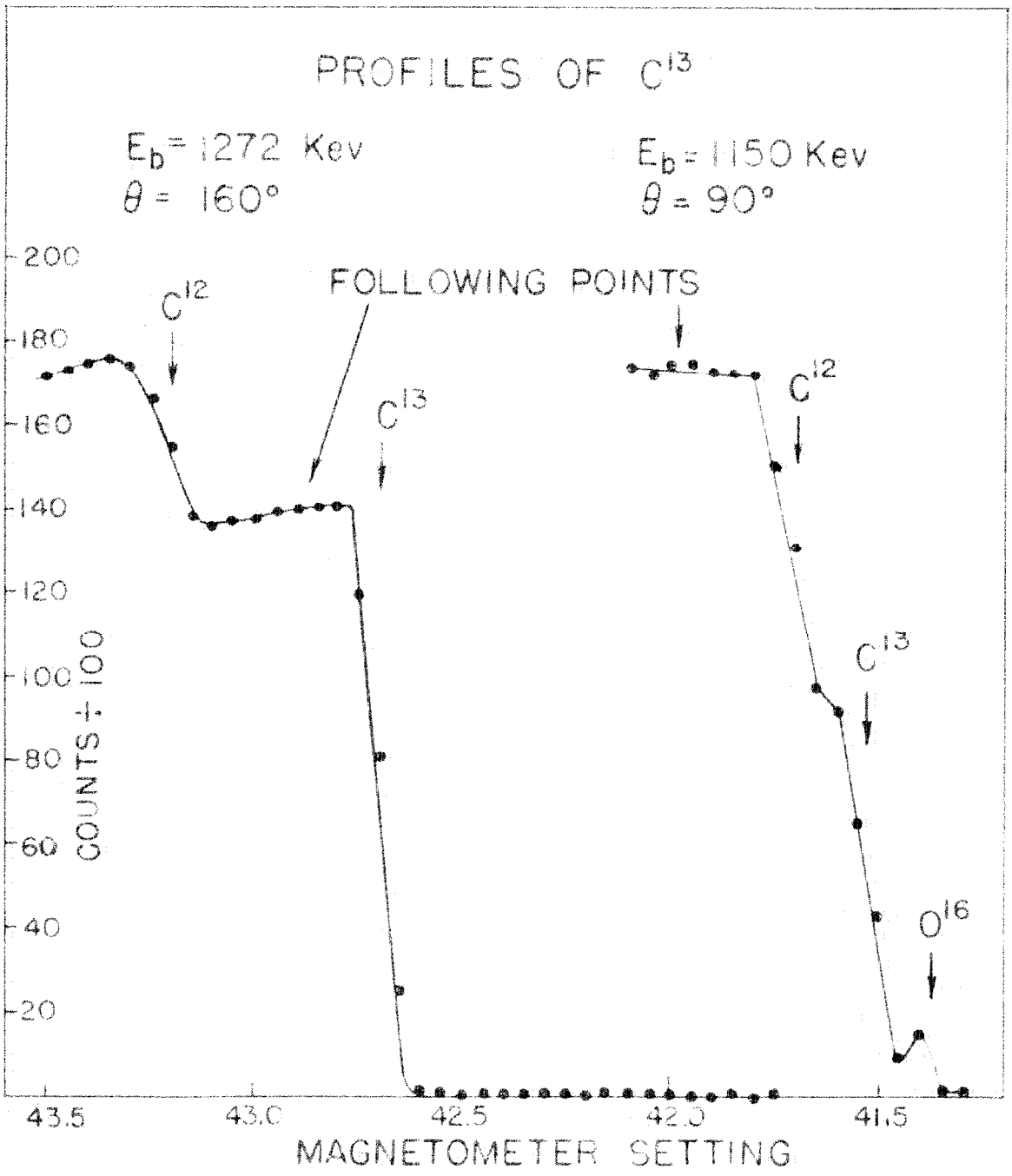
PROFILES OF C13
Eb = 1272 Kev
θ = 160°
Eb = 1150 Kev
θ = 90°
FOLLOWING POINTS
C12
C13
C12
C13
O16
200
180
160
140
120
100
80
60
40
20
COUNTS ÷ 100
43.5
43.0
42.5
42.0
41.5
MAGNETOMETER SETTING

FIGURE 7

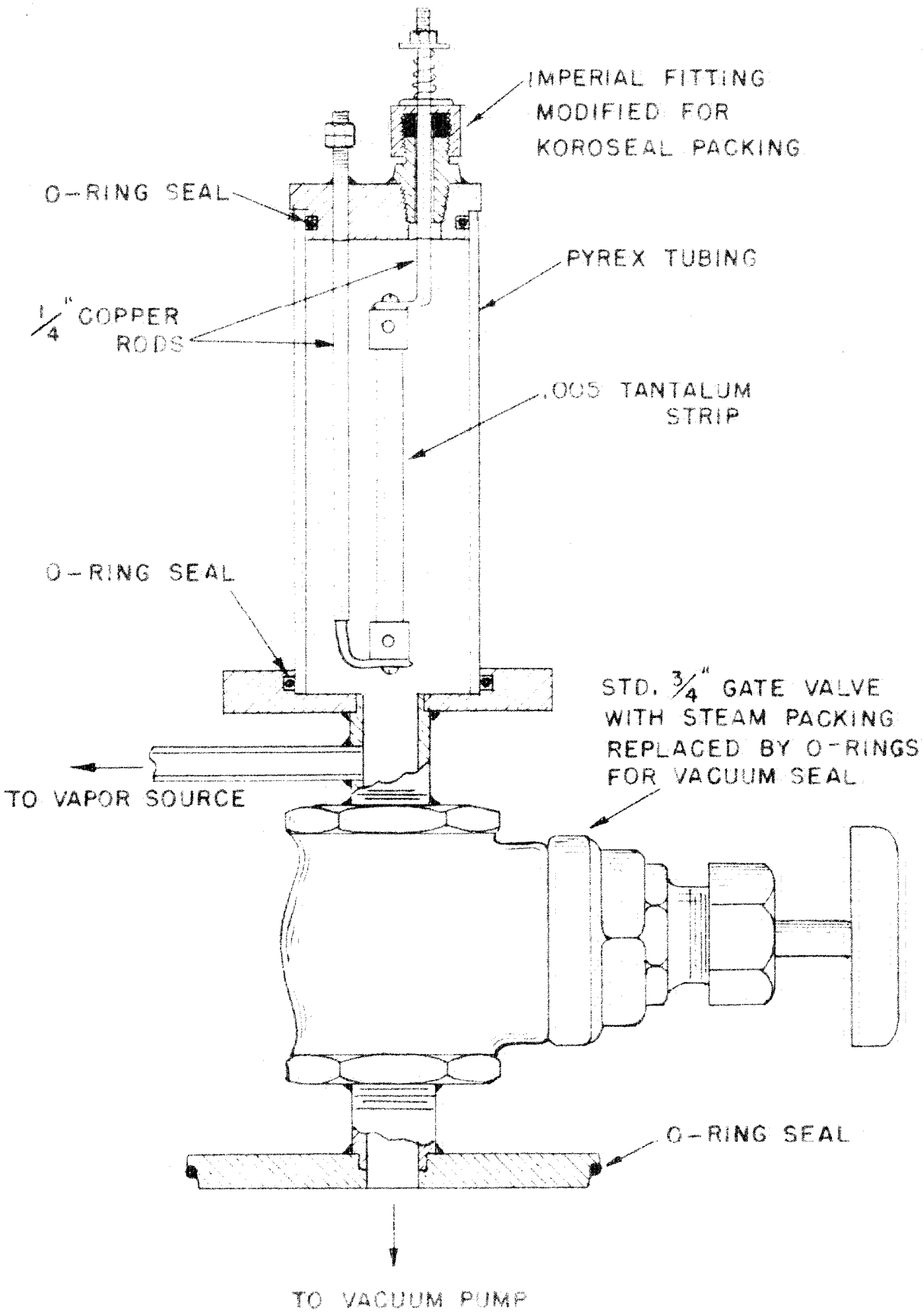
IMPERIAL FITTING
MODIFIED FOR
KOROSEAL PACKING
O-RING SEAL
PYREX TUBING
1/4" COPPER
RODS
.005 TANTALUM
STRIP
O-RING SEAL
STD. 3/4" GATE VALVE
WITH STEAM PACKING
REPLACED BY O-RINGS
FOR VACUUM SEAL
TO VAPOR SOURCE
O-RING SEAL
TO VACUUM PUMP

FIGURE 8

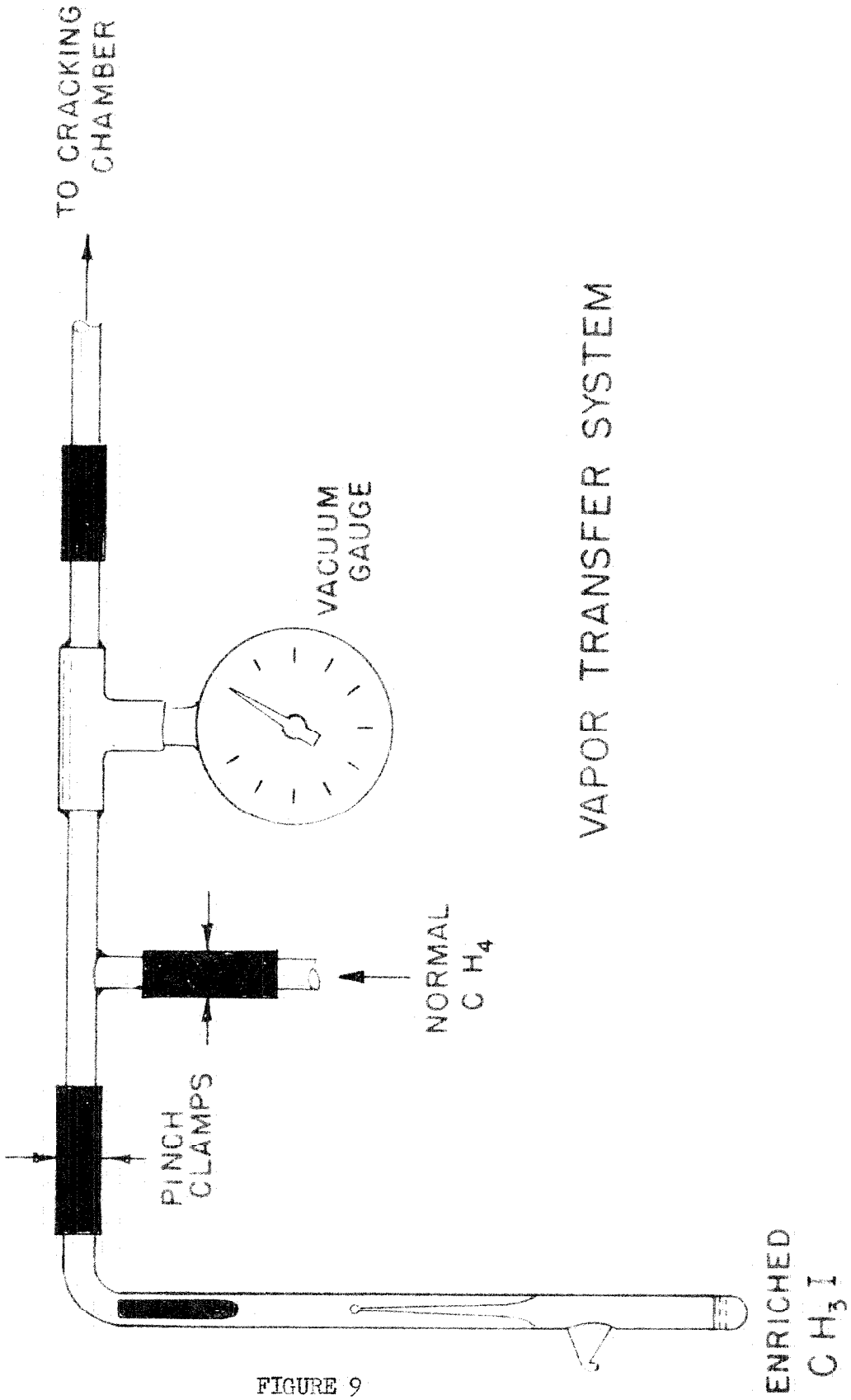
TO CRACKING CHAMBER
VACUUM GAUGE
VAPOR TRANSFER SYSTEM
NORMAL CH_4
PINCH CLAMPS
ENRICHED CH_3I

FIGURE 9

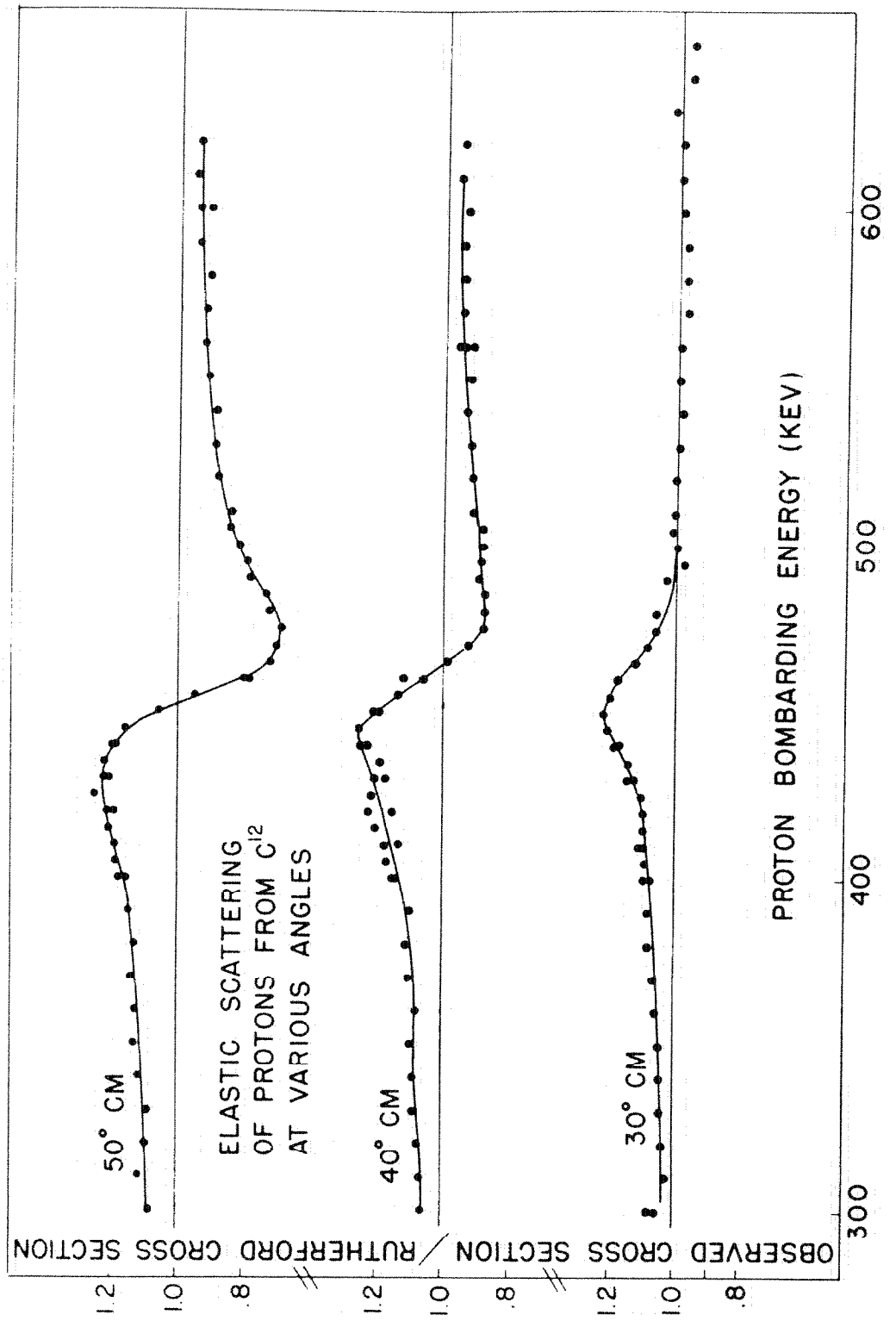
ELASTIC SCATTERING
OF PROTONS FROM C12
AT VARIOUS ANGLES
50° CM
40° CM
30° CM
RUTHERFORD CROSS SECTION
OBSERVED CROSS SECTION
PROTON BOMBARDING ENERGY (KEV)
300
400
500
600
.8
1.0
1.2

FIGURE 10

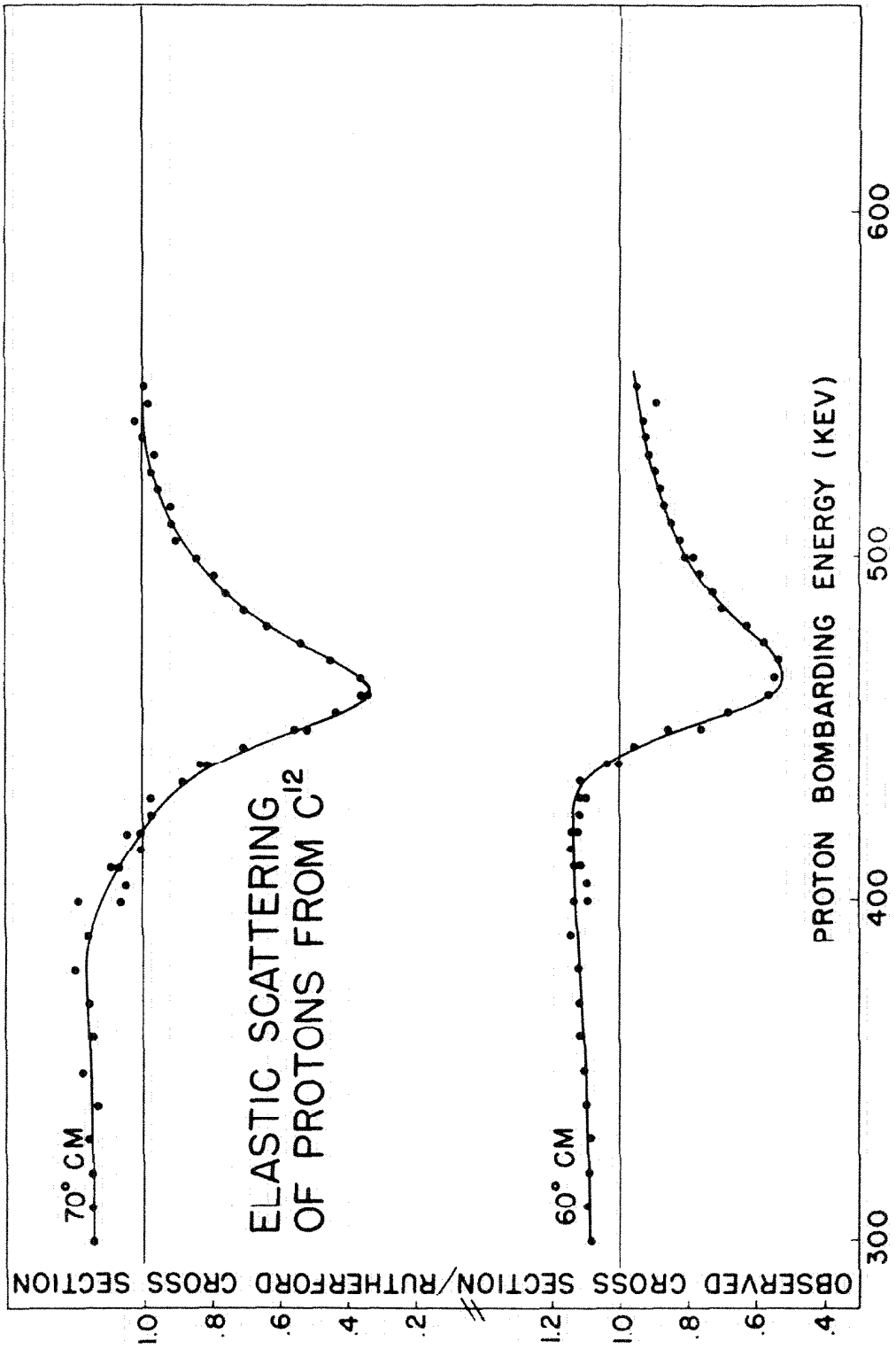
ELASTIC SCATTERING
OF PROTONS FROM C12
70° CM
60° CM
OBSERVED CROSS SECTION/RUTHERFORD CROSS SECTION
PROTON BOMBARDING ENERGY (KEV)
1.0
.8
.6
.4
.2
1.2
1.0
.8
.6
.4
300
400
500
600

FIGURE 11

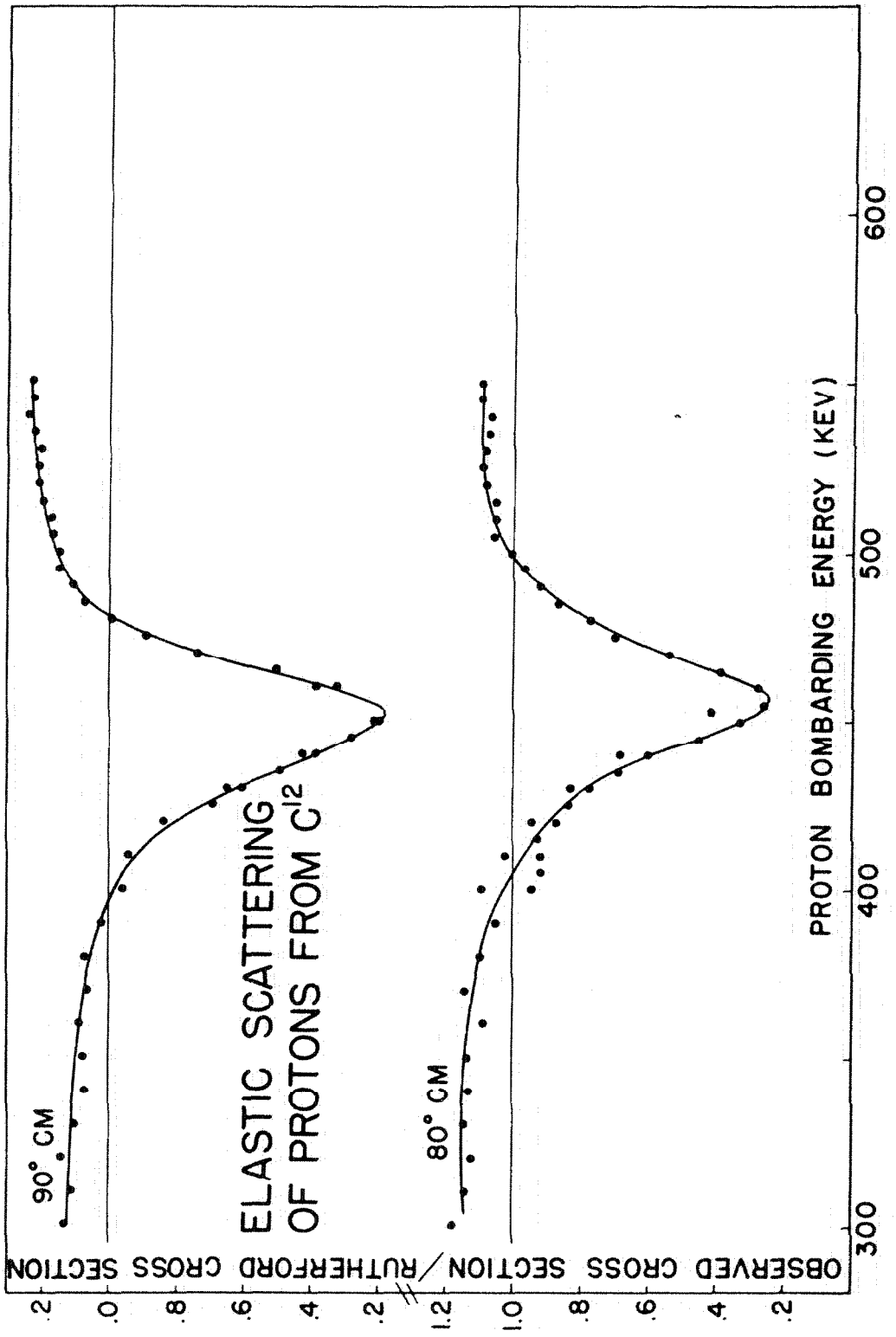
ELASTIC SCATTERING
OF PROTONS FROM C12
90° CM
80° CM
OBSERVED CROSS SECTION / RUTHERFORD CROSS SECTION
PROTON BOMBARDING ENERGY (KEV)
.2
.0
.8
.6
.4
.2
1.2
1.0
.8
.6
.4
.2
300
400
500
600

FIGURE 12

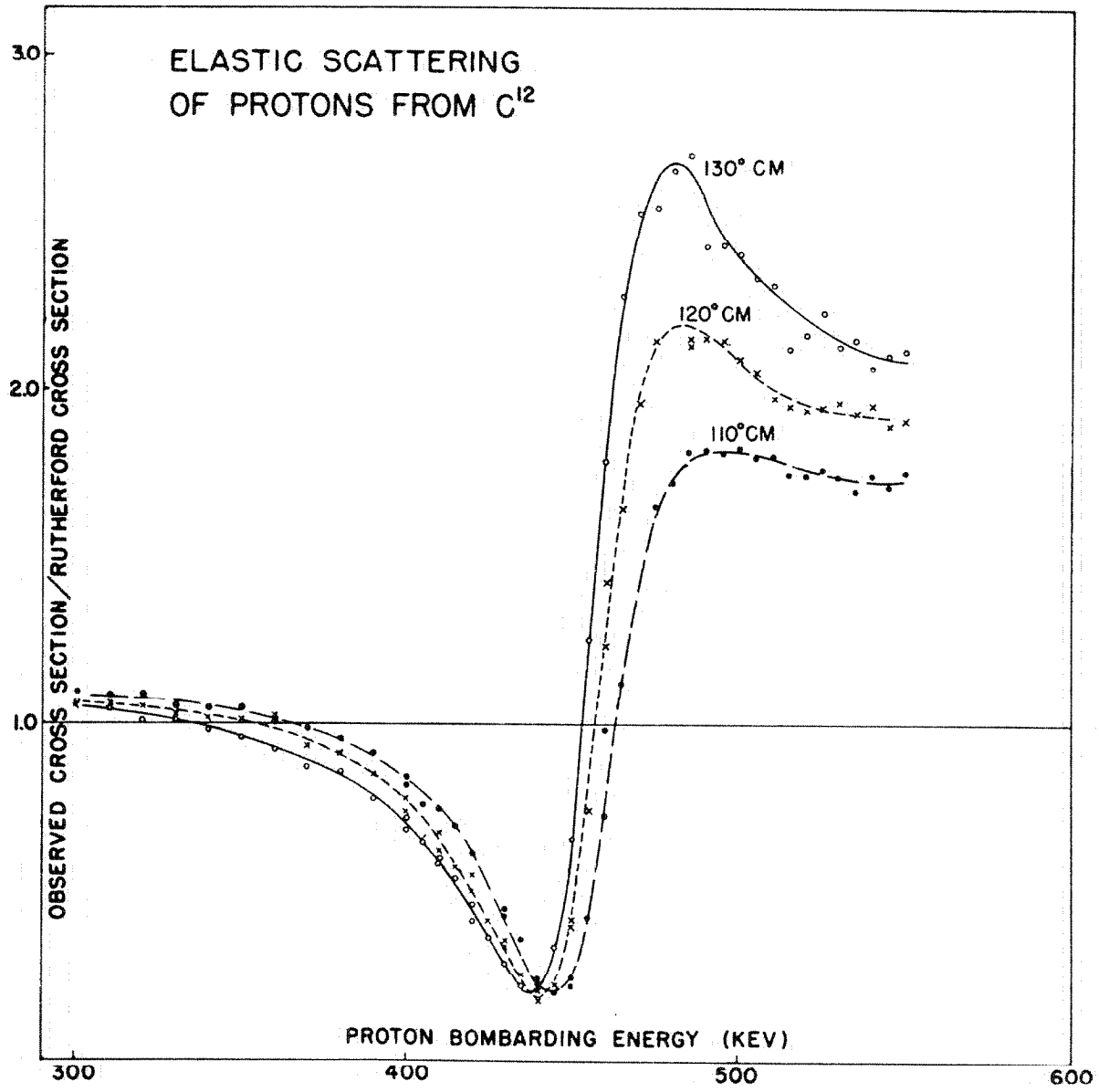
ELASTIC SCATTERING
OF PROTONS FROM C12
130° CM
120° CM
110° CM
OBSERVED CROSS SECTION/RUTHERFORD CROSS SECTION
3.0
2.0
1.0
PROTON BOMBARDING ENERGY (KEV)
300
400
500
600

FIGURE 13

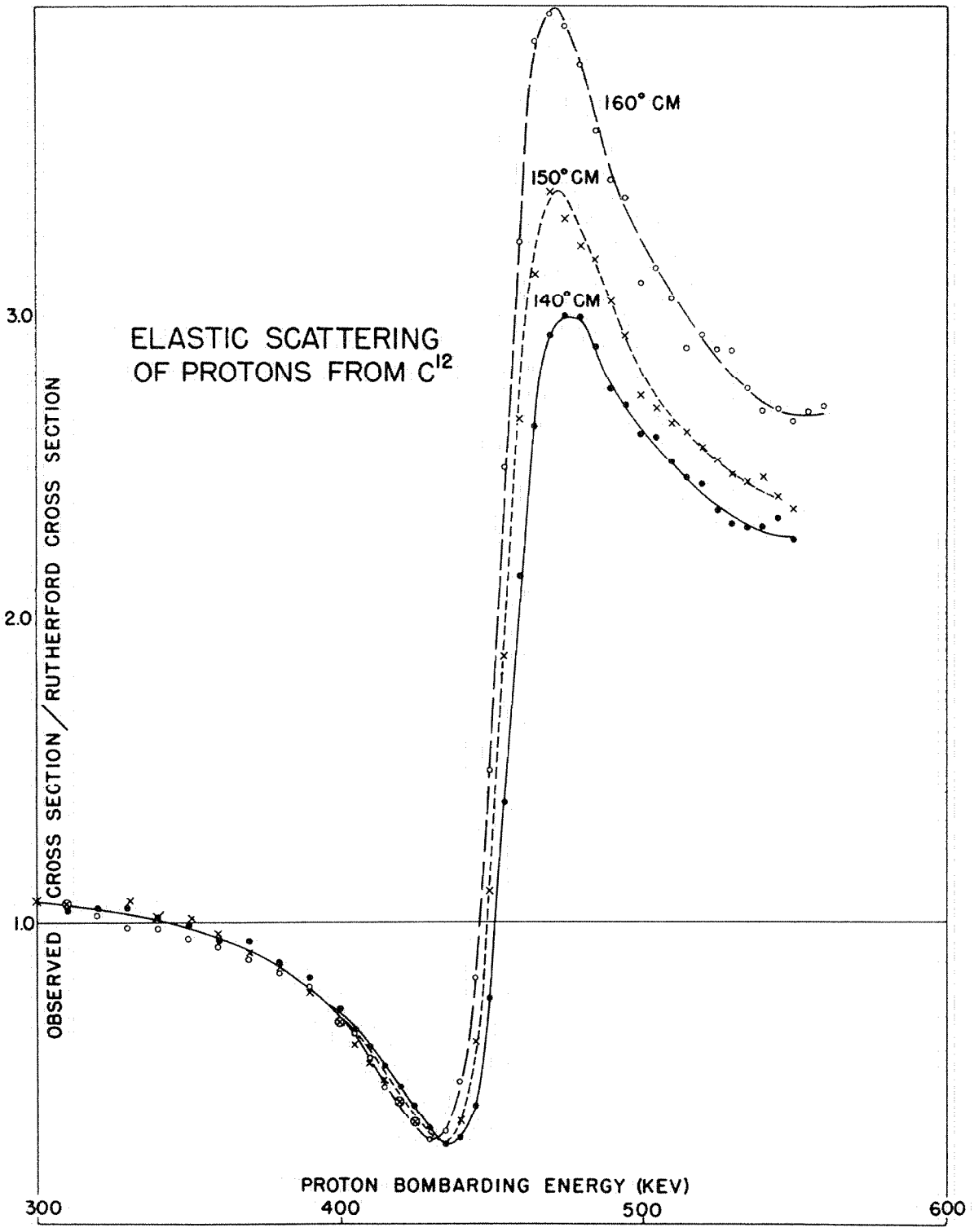
ELASTIC SCATTERING
OF PROTONS FROM C12
160° CM
150° CM
140° CM
OBSERVED CROSS SECTION / RUTHERFORD CROSS SECTION
3.0
2.0
1.0
PROTON BOMBARDING ENERGY (KEV)
300
400
500
600

FIGURE 14

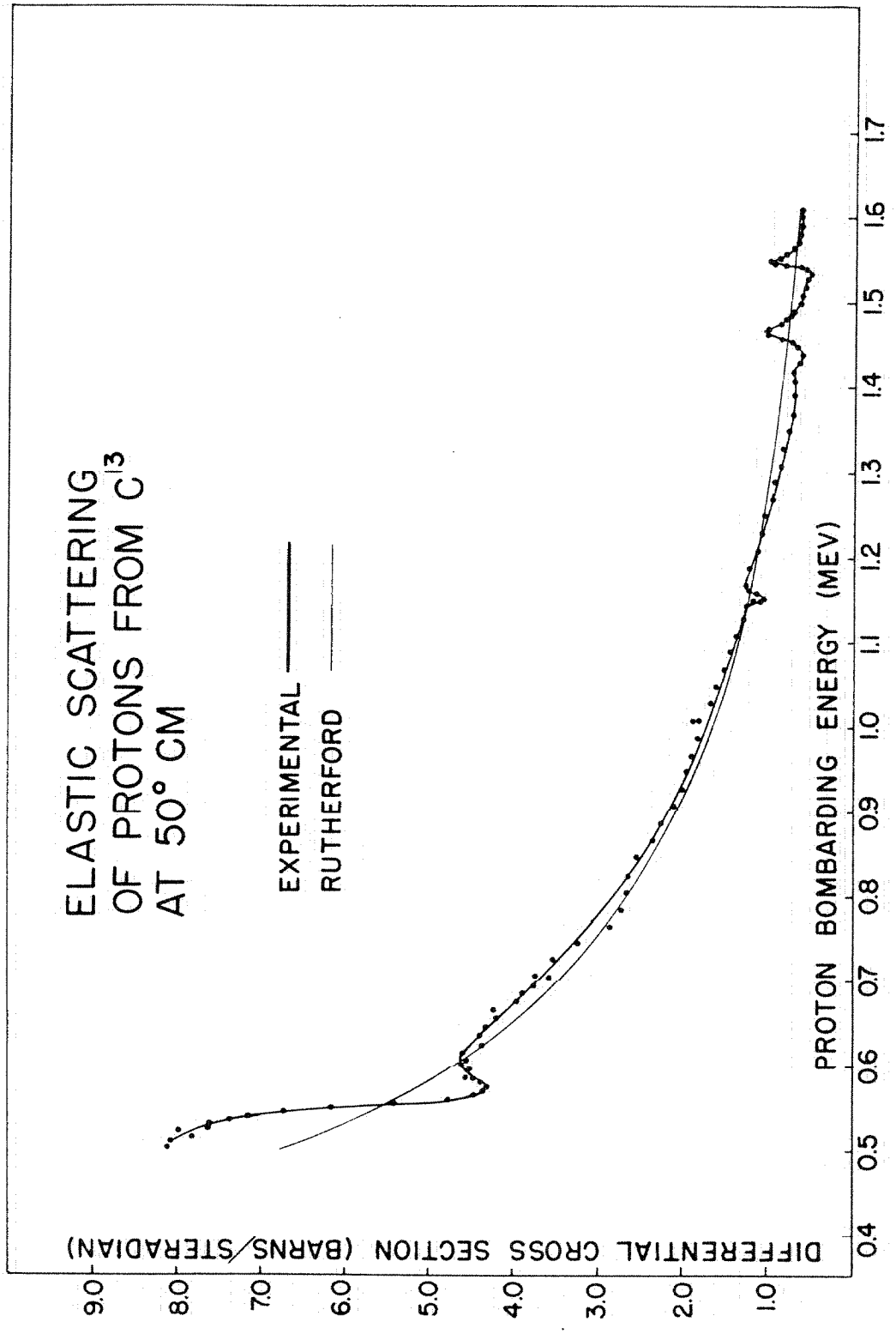
ELASTIC SCATTERING
OF PROTONS FROM C^{13}
AT 50° CM
EXPERIMENTAL
RUTHERFORD
DIFFERENTIAL CROSS SECTION (BARNS/STERADIAN)
PROTON BOMBARDING ENERGY (MEV)
9.0
8.0
7.0
6.0
5.0
4.0
3.0
2.0
1.0
0.4
0.5
0.6
0.7
0.8
0.9
1.0
1.1
1.2
1.3
1.4
1.5
1.6
1.7

FIGURE 15

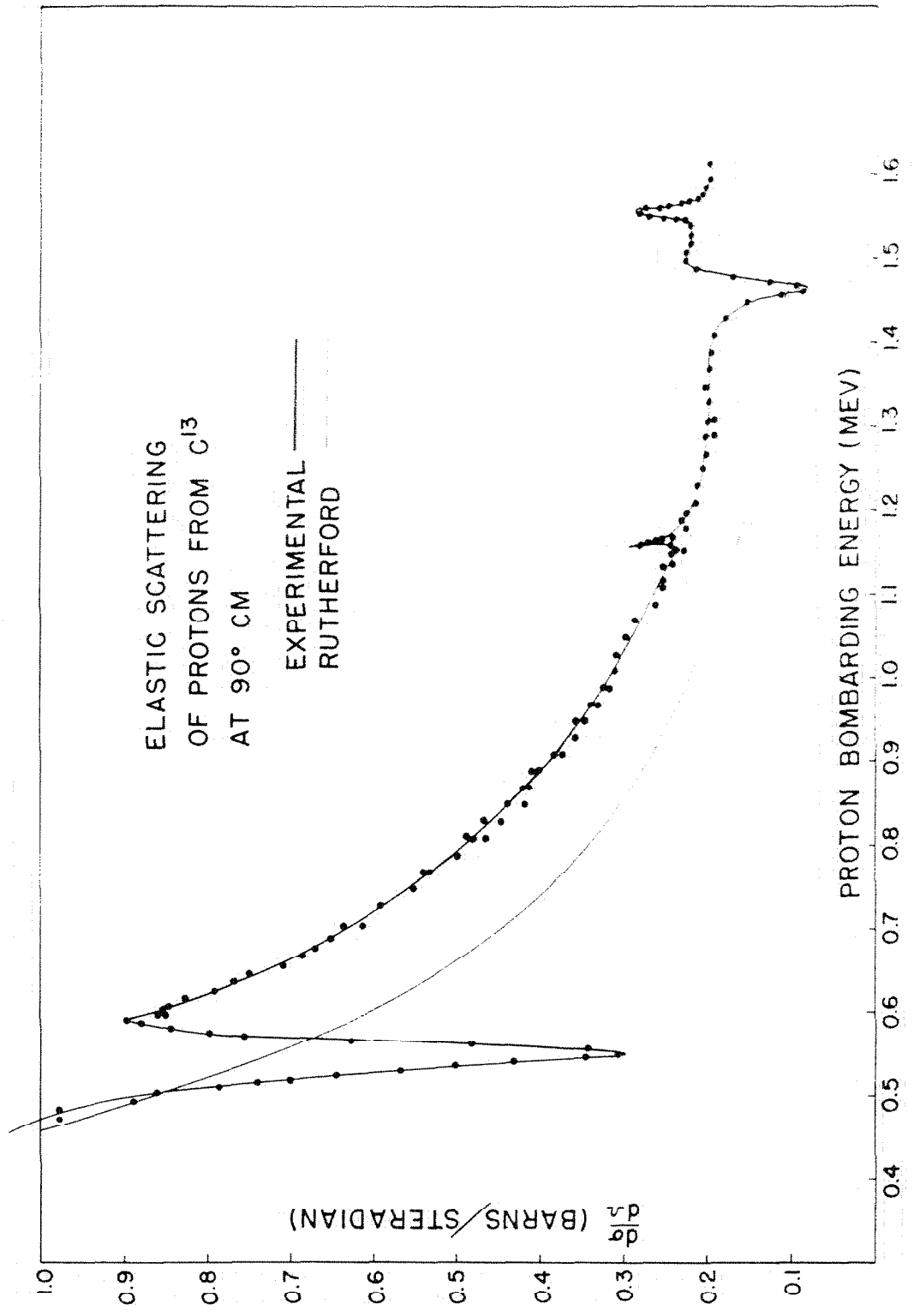
ELASTIC SCATTERING
OF PROTONS FROM C^{13}
AT 90° CM
EXPERIMENTAL
RUTHERFORD
$\frac{d\sigma}{d\Omega}$ (BARNS/STERADIAN)
PROTON BOMBARDING ENERGY (MEV)
1.0
0.9
0.8
0.7
0.6
0.5
0.4
0.3
0.2
0.1
0.4
0.5
0.6
0.7
0.8
0.9
1.0
1.1
1.2
1.3
1.4
1.5
1.6

FIGURE 16

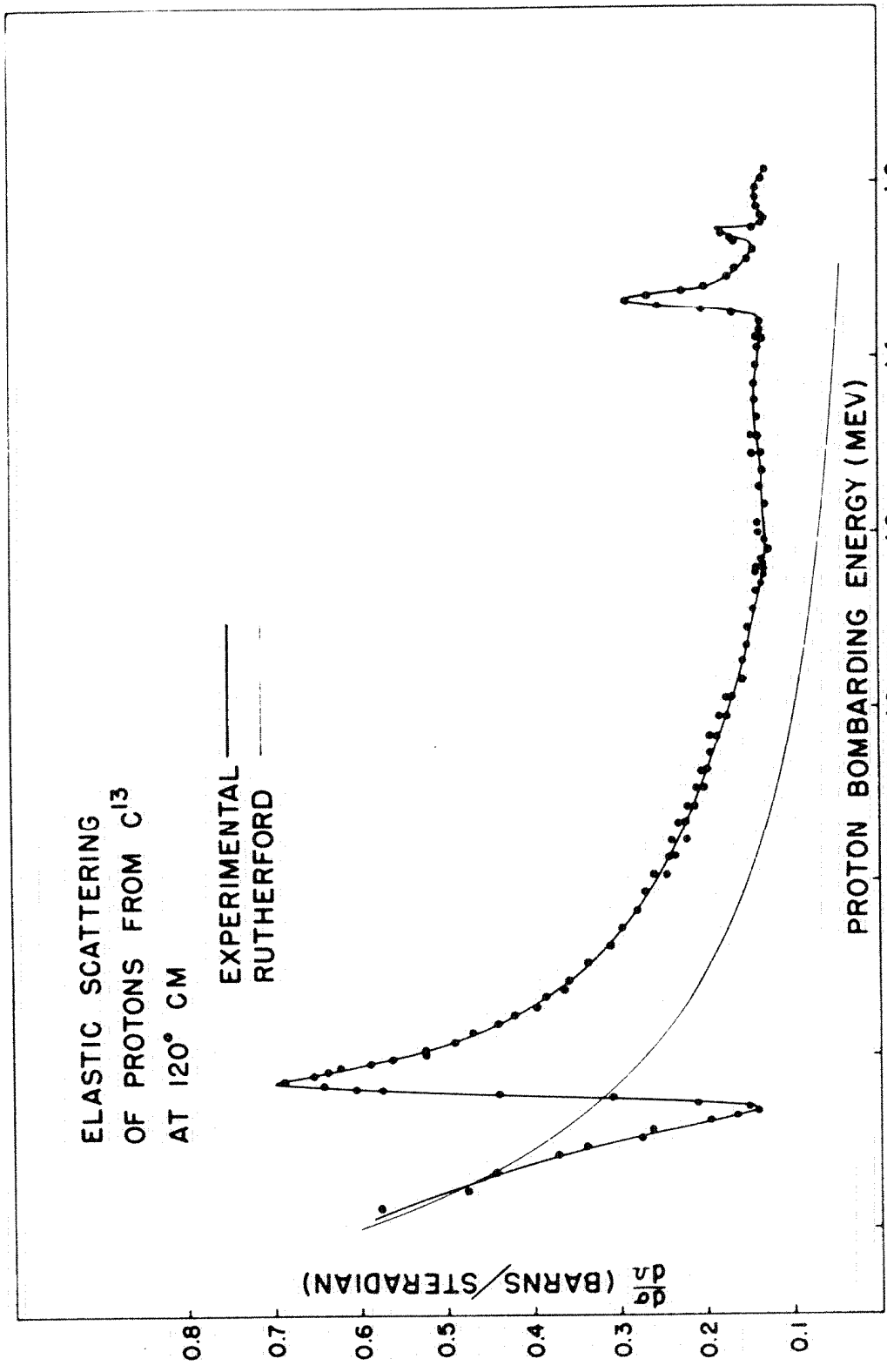
ELASTIC SCATTERING
OF PROTONS FROM C13
AT 120° CM
EXPERIMENTAL
RUTHERFORD
dσ/dΩ (BARNS/STERADIAN)
PROTON BOMBARDING ENERGY (MEV)
0.1
0.2
0.3
0.4
0.5
0.6
0.7
0.8
0.4
0.6
0.8
1.0
1.2
1.4
1.6

FIGURE 17

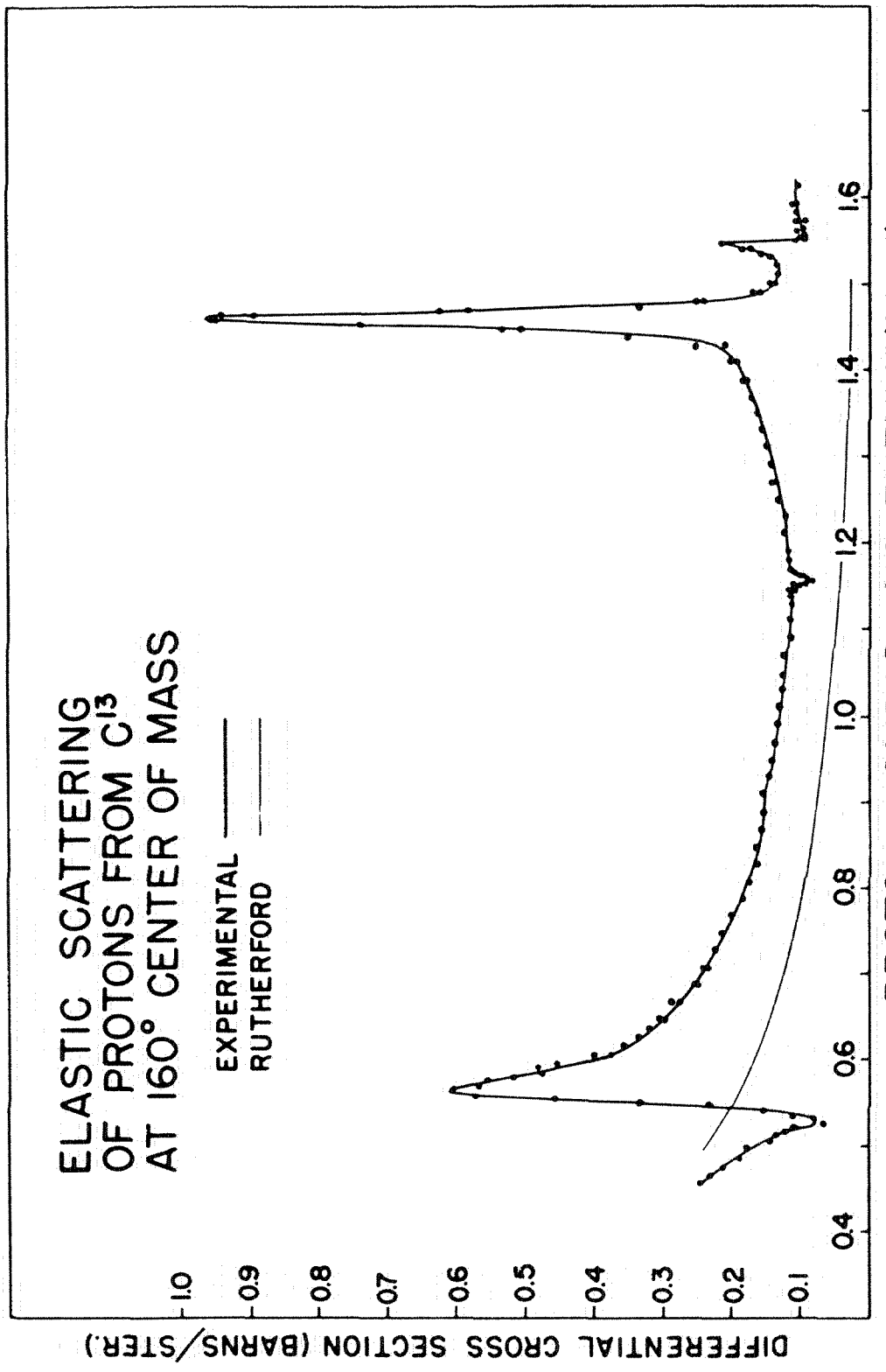
ELASTIC SCATTERING
OF PROTONS FROM C13
AT 160° CENTER OF MASS
EXPERIMENTAL
RUTHERFORD
DIFFERENTIAL CROSS SECTION (BARNS/STER.)
PROTON BOMBARDING ENERGY (MEV)
0.1
0.2
0.3
0.4
0.5
0.6
0.7
0.8
0.9
1.0
0.4
0.6
0.8
1.0
1.2
1.4
1.6

FIGURE 18

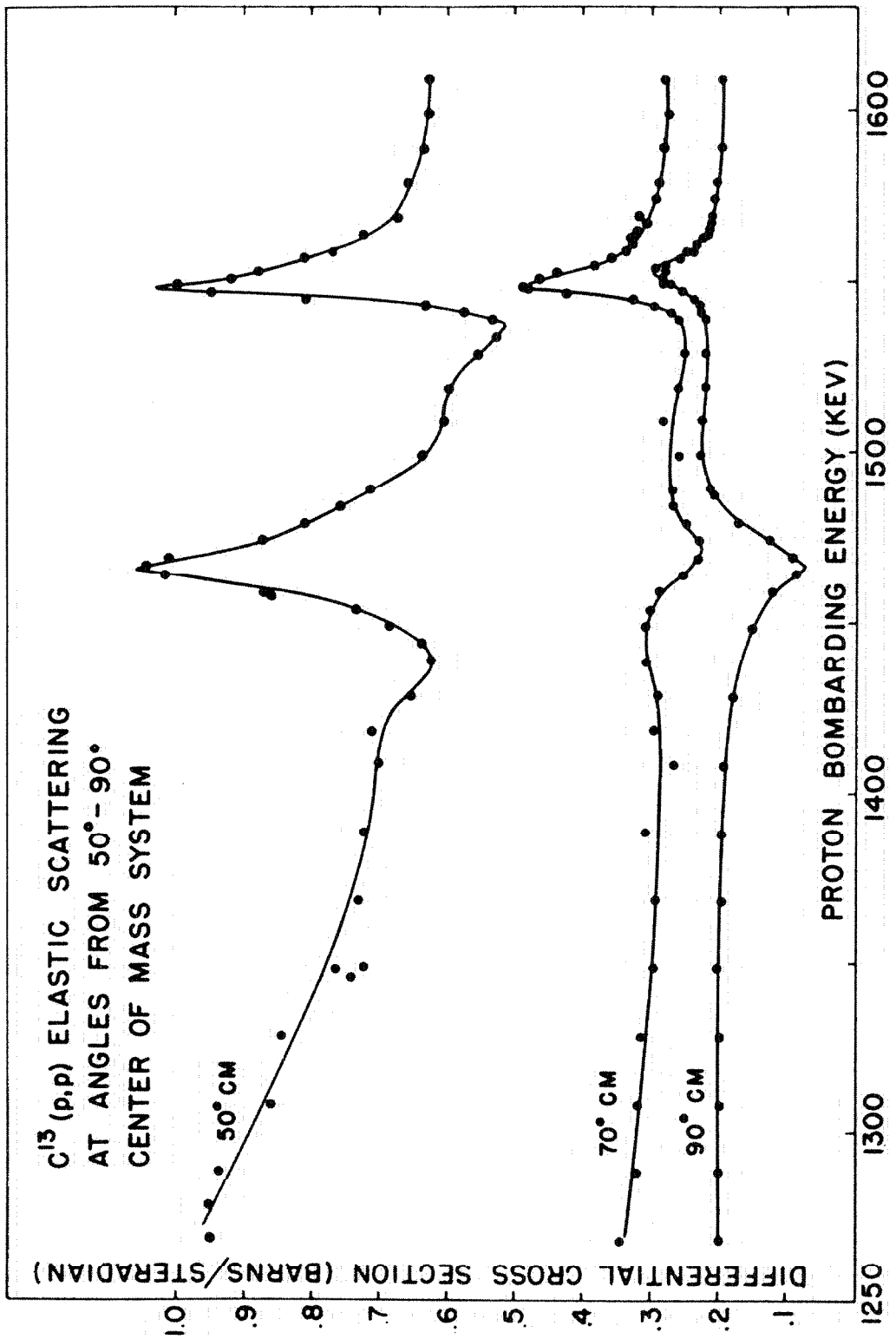
C13(p,p) ELASTIC SCATTERING
AT ANGLES FROM 50°-90°
CENTER OF MASS SYSTEM
50° CM
70° CM
90° CM
DIFFERENTIAL CROSS SECTION (BARNS/STERADIAN)
PROTON BOMBARDING ENERGY (KEV)
1.0
.9
.8
.7
.6
.5
.4
.3
.2
.1
1250
1300
1400
1500
1600

FIGURE 19

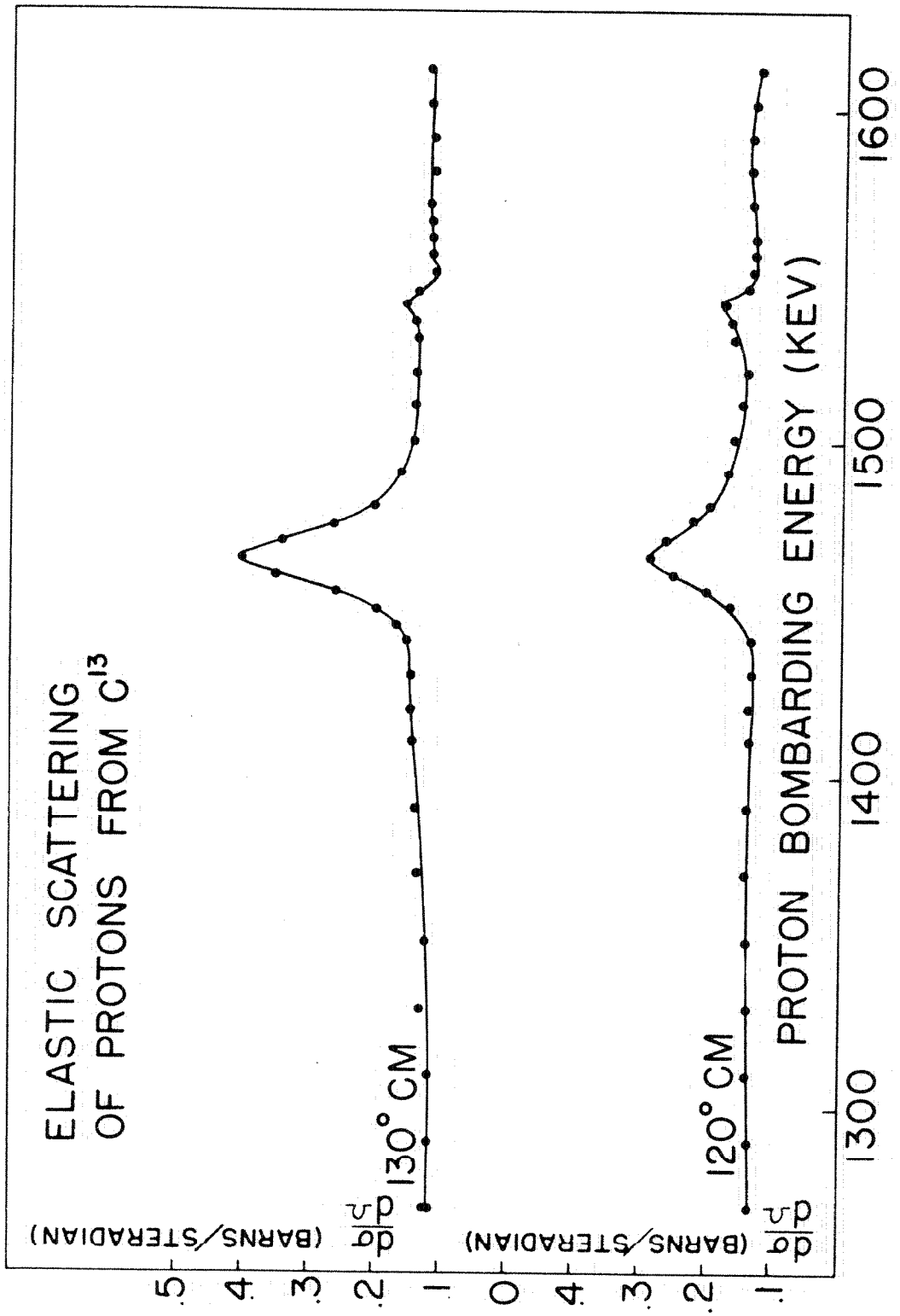
ELASTIC SCATTERING
OF PROTONS FROM C13
130° CM
120° CM
dσ/dΩ (BARNS/STERADIAN)
PROTON BOMBARDING ENERGY (KEV)
1300
1400
1500
1600
0
1
2
3
4
5

FIGURE 20

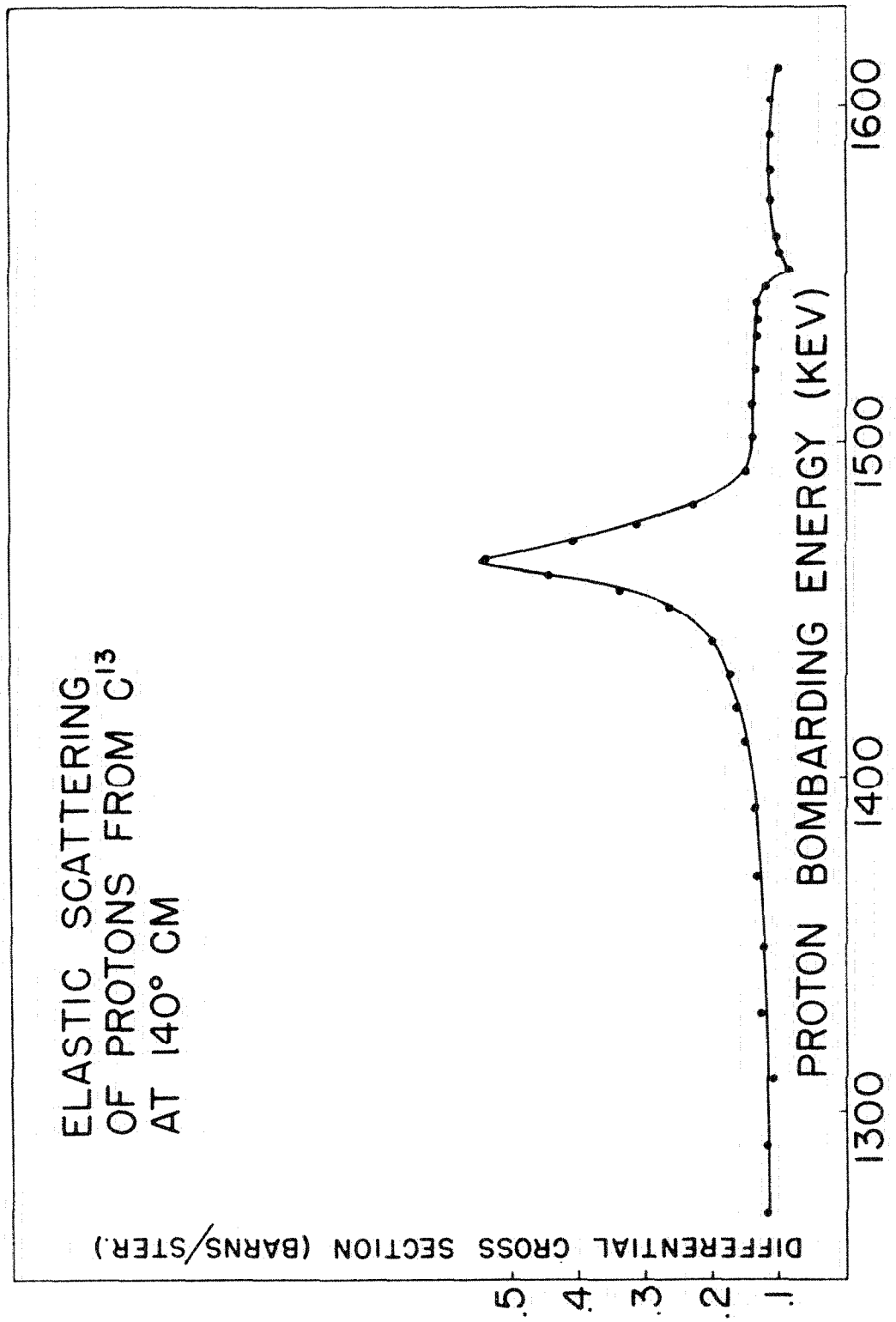
ELASTIC SCATTERING
OF PROTONS FROM C^{13}
AT 140° CM
DIFFERENTIAL CROSS SECTION (BARNS/STER.)
1
2
3
4
5
1300
1400
1500
1600
PROTON BOMBARDING ENERGY (KEV)

FIGURE 21

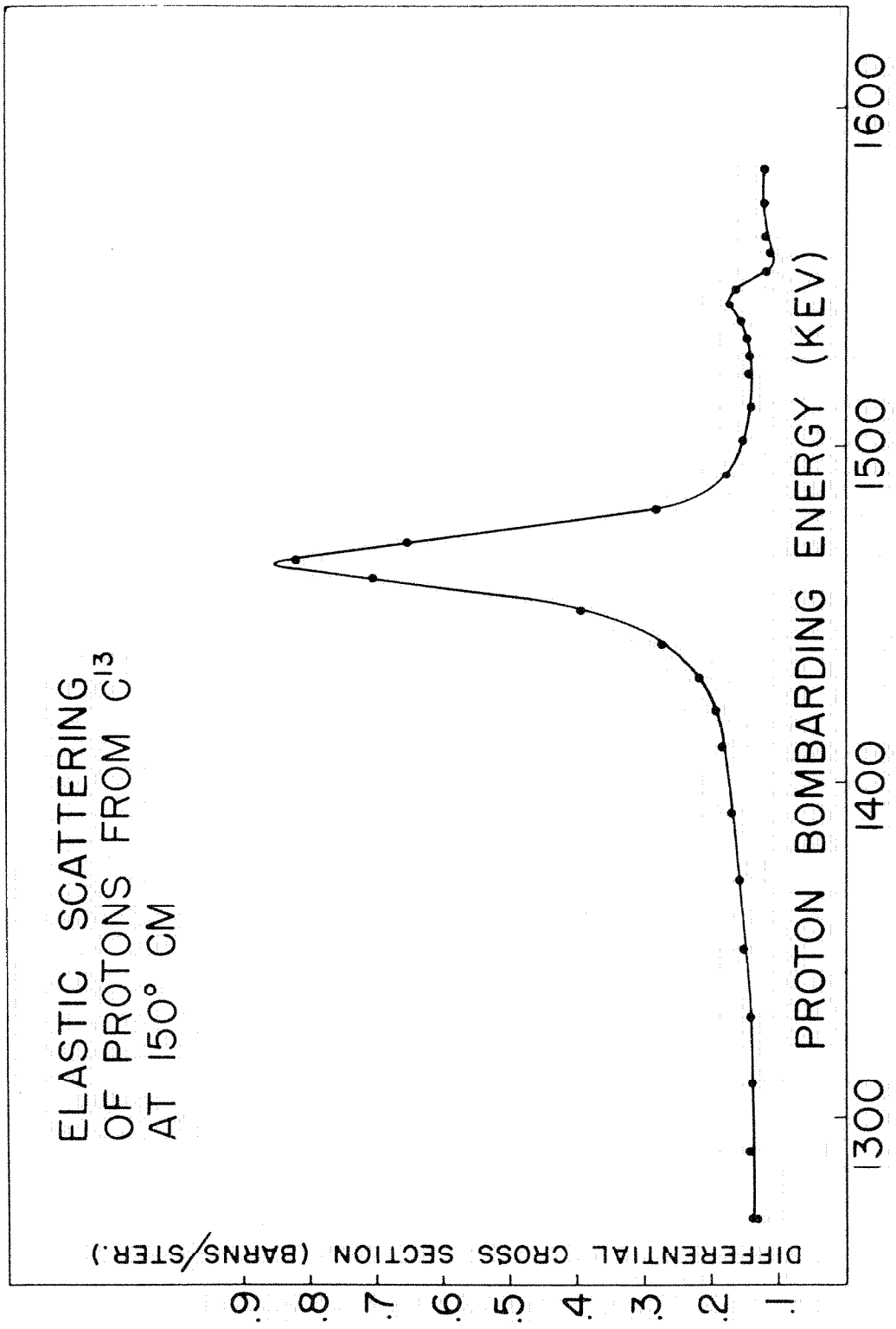
ELASTIC SCATTERING
OF PROTONS FROM C^{13}
AT 150° CM
DIFFERENTIAL CROSS SECTION (BARNS/STER.)
.1
.2
.3
.4
.5
.6
.7
.8
.9
1300
1400
1500
1600
PROTON BOMBARDING ENERGY (KEV)

FIGURE 22

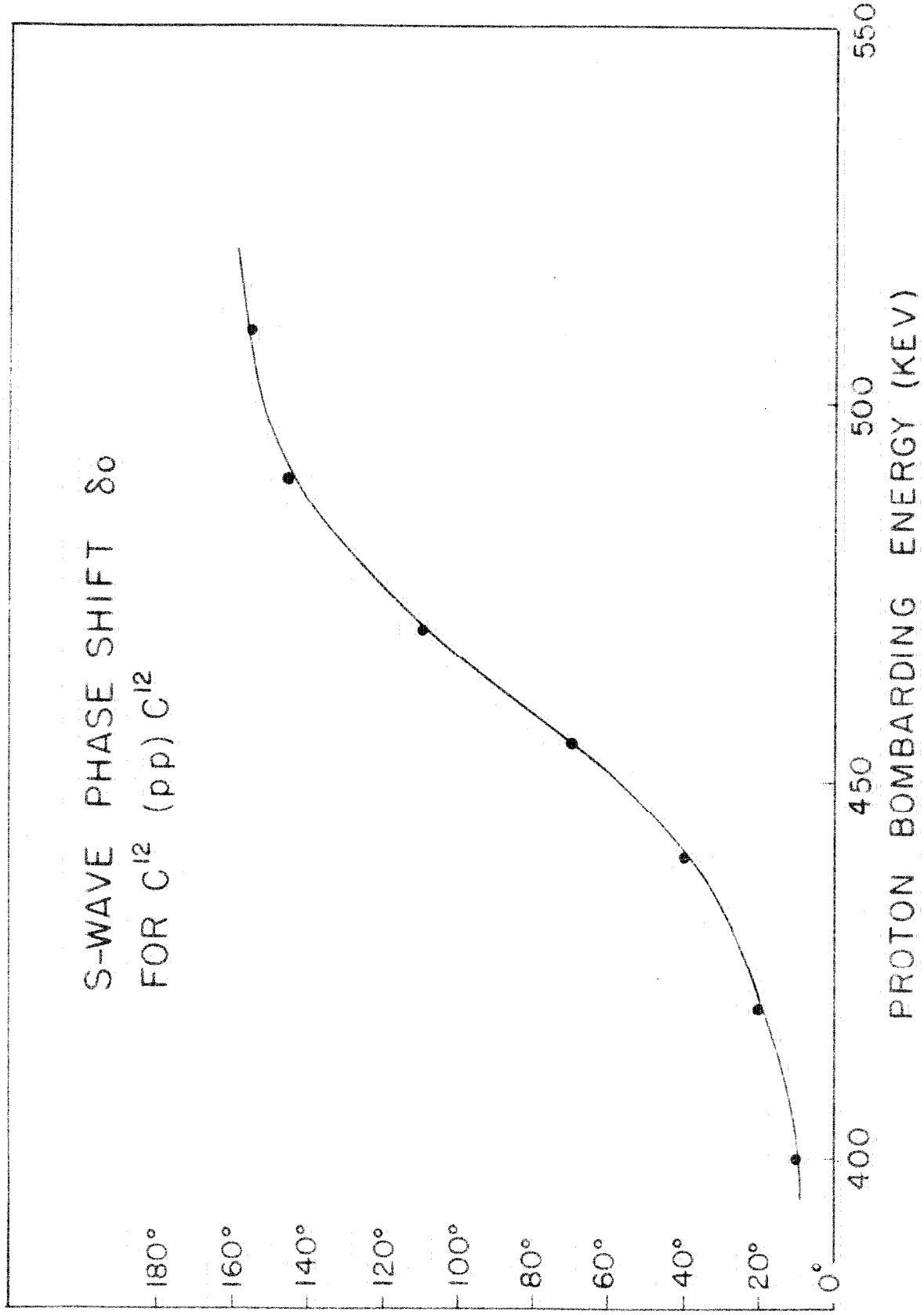
S-WAVE PHASE SHIFT δo
FOR C12 (p p) C12
180°
160°
140°
120°
100°
80°
60°
40°
20°
0°
400
450
500
550
PROTON BOMBARDING ENERGY (KEV)

FIGURE 23